Eddy-Mean Flow interactions in the Along-Stream Development of a Western Boundary Current Jet: An Idealized Model Study

Eddy-Mean Flow Interactions in the Along-Stream Development of a Western Boundary Current Jet: An Idealized Model Study

STEPHANIE WATERMAN*

Massachusetts Institute of Technology–Woods Hole Oceanographic Institution Joint Program, Woods Hole, Massachusetts

STEVEN R. JAYNE

Woods Hole Oceanographic Institution, Woods Hole, Massachusetts

(Manuscript received 1 April 2010, in final form 17 December 2010)

ABSTRACT

A theoretical study on the role of eddy-mean flow interactions in the time-mean dynamics of a zonally evolving, unstable, strongly inertial jet in a configuration and parameter regime that is relevant to oceanic western boundary current (WBC) jets is described. Progress is made by diagnosing the eddy effect on the time-mean circulation, examining the mechanism that permits the eddies to drive the time-mean recirculation gyres, and exploring the dependence of the eddy effect on system parameters.

It is found that the nature of the eddy-mean flow interactions in this idealized configuration is critically dependent on along-stream position, in particular relative to the along-stream evolving stability properties of the time-mean jet. Just after separation from the western boundary, eddies act to stabilize the jet through downgradient fluxes of potential vorticity (PV). Downstream of where the time-mean jet has (through the effect of the eddies) been stabilized, eddies act to drive the time-mean recirculations through the mechanism of an upgradient PV flux. This upgradient flux is permitted by an eddy enstrophy convergence downstream of jet stabilization, which results from the generation of eddies in the upstream region where the jet is unstable, the advection of that eddy activity along stream by the jet, and the dissipation of the eddies in the region downstream of jet stabilization. It is in this region of eddy decay that eddies drive the time-mean recirculations through the mechanism of nonlinear eddy rectification, resulting from the radiation of waves from a localized region. It is found that similar mechanisms operate in both barotropic and baroclinic configurations, although differences in the background PV gradient on which the eddies act implies that the recirculation-driving mechanism is more effective in the baroclinic case.

This study highlights the important roles that eddies play in the idealized WBC jet dynamics considered here of stabilizing the jet and driving the flanking recirculations. In the absence of eddy terms, the magnitude of the upper-ocean jet transport would be significantly less and the abyssal ocean recirculations (and their significant enhancement to the jet transport) would be missing altogether.

1. Introduction

The Gulf Stream (GS) and the Kuroshio Extension (KE) current systems are among the most energetic current systems in the World Ocean, and they are dominant features of the North Atlantic and North Pacific Oceans circulations, respectively. After separating from their respective coasts at Cape Hatteras and the Bōsō Peninsula, these western boundary currents (WBCs) turn eastward and flow into the deep ocean. Here, they are no longer constrained by topography, and they become free, inertial, unstable jets, characterized by large-amplitude meanders and pinched-off eddies. These WBC jets are of fundamental importance to the dynamics of steady basin-scale circulations as regions of enhanced exchange of potential vorticity (PV) and energy, and they act to restore global balances between forcing and dissipation. Understanding their dynamics is fundamental to improving our understanding of the ocean general circulation.

* Current affiliation: National Oceanography Centre, Southampton, and Grantham Institute for Climate Change, Imperial College London, London, United Kingdom.

Corresponding author address: Stephanie Waterman, National Oceanography Centre, Empress Dock, Southampton SO14 3ZH, United Kingdom.
E-mail: snw@alum.mit.edu

DOI: 10.1175/2010JPO4477.1

Observations indicate that eddy kinetic energy (EKE) is strongly (orders of magnitude) spatially inhomogeneous, reaching maxima in the vicinity of strong currents such as these WBC jets (Ducet and Le Traon 2001). The GS and KE regions are prime examples of this, where the meandering of the streams results in an increase in the eddy kinetic and eddy potential energies by orders of magnitude along the climatological mean path of the jet throughout the water column (Schmitz 1984; Malanotte-Rizzoli 1994; Hogg 1988; Bower and Hogg 1992). Given such high levels of eddy activity in these regions, our description of WBC jet dynamics requires an understanding of the effects of this eddy variability.

An investigation of eddy-mean flow interactions in WBC jets is important because eddies potentially play an important role in the dynamics of these jet systems. Through their fluxes of momentum and vorticity, eddies can be significant in determining the character of the mean jet (its mean strength, structure, and stability properties). Acting not only as a source of dissipation, eddies can also act as a driving force through nonlinear eddy–eddy and eddy-mean flow interactions (Thompson 1977, 1978; Dewar and Bane 1989; Hogg 1992; Watts et al. 1995). Eddies play a potential role in driving recirculations, the phenomenon through which the along-stream transport of the separated jet is increased several-fold by the development of flanking, weakly depth-dependent gyres (Richardson 1985; Schmitz and McCartney 1993). Furthermore, eddy variability appears to also play a role in coupling the strong motions in these baroclinic jets to deep abyssal circulations, driving the deep recirculation gyres (Hogg 1983, 1985, 1993) and potentially acting back on the upper jet, influencing its speed and direction (Cronin and Watts 1996; Cronin 1996). Finally, eddies may play a role in modulating the low-frequency variability in jet transport, the degree of meandering intensity and EKE, and the recirculation structure that these systems exhibit (Lee and Cornillon 1995; Qui 1995; Kelly et al. 1996). There are many possible explanations for the source of this variability ranging from external (e.g., atmospheric) forcing (Qui 1995) to multiple state equilibria associated with highly inertial dynamics (McCalpin and Haidvogel 1996; Berloff and Meacham 1998; Primeau 1998; Berloff and McWilliams 1999; Meacham 2000), but eddy effects may be important as well. For example, Spall (1996) and Qui (2000) have shown that the process of eddies fluxing PV away from the detached jet can lead to natural low-frequency oscillations (i.e., even without atmospheric coupling) in recirculation gyre systems.

Given the importance of WBC jets, work on the subject of their dynamics has had a long history. Theoretical studies that lay the foundation onto which the work described here is built can be thought of dividing into the following three categories:

(i) inertial theories in which time-mean recirculation gyres can arise from the steady-state time-mean advection of PV alone (e.g., Fofonoff 1954; Marshall and Nurser 1986; Greatbatch 1987; Cessi 1990)
(ii) eddy-driven theories in which the effects of a directly prescribed vorticity forcing generates time-mean rectified flows through eddy-mean flow and eddy–eddy interactions (e.g., Starr 1968; Whitehead 1975; Haidvogel and Rhines 1983; Cessi et al. 1987; Malanotte-Rizzoli et al. 1995; Berloff 2005; Waterman and Jayne 2010, manuscript submitted to *J. Phys. Oceanogr.*); and
(iii) unstable jet studies in which the generation of time-mean recirculations arise from unstable jets in which eddy effects (arising from jet instabilities) and inertial effects can both play a role (e.g., Spall 1994; Jayne et al. 1996; Beliakova 1998; Jayne and Hogg 1999; Mizuta 2010)

Collectively, these approaches demonstrate that recirculations can arise from the steady-state inertial terms, the rectification of eddy fluxes, or potentially both. Steady-state inertial theories show that closed recirculation gyres are steady solutions to the nonlinear equations of motion forced by a balance between the inertial term (the mean advection of PV) and dissipation. At the same time, time-dependent numerical simulations demonstrate that zonal flows and closed recirculations can be generated solely from rectification effects through nonlinear eddy-mean flow and eddy–eddy interactions. Finally, rectified mean flows can also result from forcing by an unstable jet. In this case, mean recirculations to the north and south of the jet are produced by waves or eddies generated by the jet; these act to smooth the PV anomalies associated with the jet, and in the process produce homogenized regions in which essentially inertial recirculations can develop. It is interesting that recirculations generated in this way in barotropic models are able to predict recirculation strength quite accurately in spite of their reliance solely on the barotropic instability mechanism.

Despite the highly variable, zonally evolving, strongly inertial and strongly baroclinic nature of WBC jet systems, thus far model configurations in which all of these components can interact and compete remain relatively unexplored. In previous work, theoretical studies of inertial effects in WBC jets have tended to be in steady (time independent) frameworks, with eddies parameterized as a downgradient diffusion of PV (Marshall and Nurser 1986; Greatbatch 1987; Cessi 1990). Hence, they fail to address the relative importance of inertial versus eddy effects, both

of which are likely to be important in the oceanic system. At the same time, studies on the role of eddies in these regimes have largely been devoid of the consideration of jet inertial effects (Haidvogel and Rhines 1983; Cessi et al. 1987; Malanotte-Rizzoli et al. 1995; Berloff 2005). In this case, there is an inadequate connection between the prescribed forcing and the system's intrinsic dynamics. Exceptions are the work of Jayne et al. (1996), Beliakova (1998), Jayne and Hogg (1999), and Mizuta (2010), studies that have addressed several of the issues related to the generation and maintenance of recirculations by a free inertial jet in barotropic, equivalent barotropic, and baroclinic systems. These studies however are limited to zonally symmetric configurations and a focus on low-frequency variability and multiple dynamical regimes in the case of the work of Beliakova (1998) and to barotropic or equivalent barotropic dynamics without focus on the eddy-mean flow interaction mechanisms in the case of the studies of Jayne et al. (1996) and Jayne and Hogg (1999).

The work discussed here attempts to extend our theoretical understanding of the role of eddy variability in the time-mean dynamics of a zonally evolving, strongly inertial, baroclinic, unstable jet in a configuration and parameter regime that is relevant to the GS and KE jet systems. It can be considered an extension of the work of Jayne et al. (1996), Jayne and Hogg (1999), and Mizuta (2010) with a view to expand our understanding of the eddy-mean flow interaction mechanisms involved and to include baroclinic dynamics (and baroclinic instability).

We address the following questions in an idealized model of a WBC jet:

(i) What is the effect of eddies on the time-mean circulation, and what mechanisms permit that effect?
(ii) How does the addition of baroclinicity and baroclinic instability change our understanding of the eddy effects in a barotropic model?
(iii) How does this effect vary with system parameters, in particular the stability properties of the WBC, which are the source of the eddy variability?

These questions are examined through the study of a numerical model of the along-stream evolution of a barotropic jet subject to barotropic instability, and a baroclinic jet (in a two-layer framework) subject to a mixed (barotropic and baroclinic) instability mechanism.

This paper is organized as follows: In section 2, we outline our approach. Here a brief, conceptual description and justification of the model setup are given. For specific details about the model configuration and the experiments performed, see the appendix. In section 3, we present a diagnosis of the eddy effect on the time-mean circulation in the barotropic case, examining the role of the eddies in stabilizing the jet and driving the time-mean recirculation gyres and exploring the mechanism that permits the eddies to drive the time-mean recirculation gyres in this configuration. In section 4, we examine the baroclinic, mixed instability case with the same objectives. Here, the nature and relative importance of eddy relative vorticity fluxes versus thickness fluxes (the two-layer model equivalent to buoyancy fluxes) is also addressed. In section 5, the dependence of the eddy effect on system parameters is discussed. Finally, in section 6, we summarize and discuss the results and evaluate their relevance to actual WBC jets by considering them in the context of past observational results.

2. Methodology

We study the role of eddy-mean flow interactions in the along-stream evolution of an idealized WBC jet using a numerical model of an unstable, boundary forced jet in an open domain. The model is quasigeostrophic, on a β plane, and fully nonlinear, with x (zonal), y (meridional), and time dependence. It is run in one- and two-layer configurations.

The model is forced at the western boundary by imposing a jet inflow directed eastward at $x = 0$ that, in the typical case, is scaled appropriate to a WBC extension jet (see Fig. 1). In the typical baroclinic case, this same jet inflow is prescribed at the western boundary in the upper layer with zero inflow prescribed at the western boundary in the lower layer, appropriate to the WBC at the point of separation from the coast when it turns eastward to enter the deep, relatively quiescent, open ocean. In the barotropic case, this inflowing jet is potentially barotropically unstable (i.e., it satisfies the Rayleigh necessary condition for instability requiring the PV gradient profile, $dQ/dy = \beta - (d^2U/dy^2)$, to change sign in the horizontal).[1] In the baroclinic case, it has the potential for both barotropic and baroclinic instability (i.e., it satisfies the two-layer model necessary condition for instability requiring the PV gradient profile to change sign either in the horizontal or in the vertical; Pedlosky 1963). In this case, the layered PV gradient profiles given by $dQ_1/dy = \beta - (d^2U_1/dy^2) + (1/S_1)(U_1 - U_2)$ and $dQ_2/dy = \beta - (d^2U_2/dy^2) + (1/S_2)(U_2 - U_1)$ have a sign reversal in both the horizontal and in the vertical in both layers (see Fig. 1, top left).[2]

[1] Here, Q is the meridional profile of the PV of the inflowing jet; β is the meridional planetary vorticity gradient; and d^2U/dy^2 is the meridional profile of the meridional gradient of the jet's relative vorticity dU/dy, where U is the meridional profile of the zonal velocity of the inflowing jet.

[2] Here, $Q_{n=1,2}$ is the meridional profile of the PV in the nth layer; $U_{n=1,2}$ is the meridional profile of the zonal velocity in the nth layer; and $S_{n=1,2}$ is the nth-layer Burger number, $S_n = (ND_n/fL)^2$. Here, N is the buoyancy frequency, D_n is the nth-layer depth, and f is the Coriolis frequency.

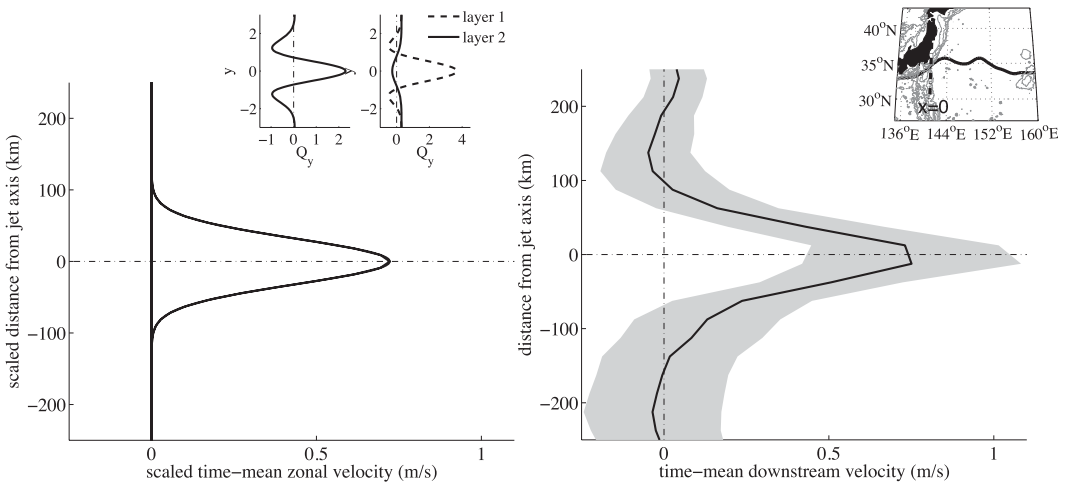

FIG. 1. (left) Inflowing jet profile for the WBC-typical model run dimensionalized according to the appropriate value of nondimensional β ($\beta = 0.05$ in this case) and (right) the synoptic mean jet profile of the Kuroshio at the point of separation from the coast. The Kuroshio profile is derived from satellite altimetry data [source: Archiving, Validation, and Interpretation of Satellite Oceanographic data (AVISO)] for the period 1992–2006. The time-mean (solid black line) and the mean ± its standard deviation (gray shading) profiles are shown. See Waterman (2009) for a description of the synoptic mean calculation. (top right) The profile is taken at a longitude of 141°E (dashed line $x = 0$), corresponding to where the time-mean Kuroshio path defined by the 2.1 sea surface height contour (solid black line) leaves the continental slope (gray contours denote bathymetry) [source: 5-minute gridded elevations/bathymetry for the world (ETOPO5)] with contour intervals of 2000-, 4000-, 6000-, and 8000-m depths}. (top right) The meridional profile of the meridional gradient of PV of the inflowing jet $\partial Q/\partial y$ for both the barotropic and baroclinic configurations used to assess the inflowing jets' stability properties.

Given that it is our intent to model the along-stream development of a free inertial jet applicable to the WBC after it has separated from the coast and entered the open ocean, we allow the jet to evolve freely in the zonal direction from the western edge of the domain. The inflowing mass must be removed from the domain at the eastern boundary, and it is important to the relevance of the model to the along-stream development of a WBC jet in the open ocean that the eastern boundary condition does not control the upstream dynamics we study. We make the upstream dynamics qualitatively insensitive to the outflow condition by making the zonal extent of the domain long relative to the zonal extent we examine (in particular, long relative to the zonal scale over which the jet broadens and becomes stable) and through a zonally broad eastern boundary sponge layer, which allows the jet to adjust to the outflow condition near the eastern boundary. For further details, please see the appendix. We note that the eastern boundary condition does have an important influence on the interior model dynamics by setting the outflowing PV structure and, as such, on how the model interior dynamics must modify the jet's PV profile between the inflow and outflow. As a consequence, for all parameter studies we fix the outflow condition and the eastern sponge layer configuration, thus restricting influence on this forcing amplitude to the inflowing jet parameters we vary. We also view parameter study results as a function of the net (inflow–outflow) PV anomaly associated with the imposed inflowing and outflowing jet profiles to explicitly recognize that this is the relevant control on the magnitude of the interior eddy PV flux divergence.

In addition to the eastern sponge layer, we also put sponge layers on the northern, southern, and western boundaries. The sponges act to prevent wave reflection back into the interior and damp basin modes and, as such, allow us to better simulate open ocean conditions. We examine the dynamics in the interior far from the northern, southern, and eastern sponge layers (for quantitative details, see the appendix) and ensure these dynamics are qualitatively insensitive to these sponge layers' extent and damping rate, thus allowing us to focus on the western boundary layer and the interior dynamics that are relevant to the WBC jet in an open ocean environment. We note that unlike the sponges on the other lateral boundaries, the sponge layer at the western boundary is an important part of the domain and dynamics we study, and our solution will be an important function of the western sponge layer extent and damping rate. The presence of the sponge layer on the western boundary also has the effect of eliminating any feedback of the recirculation strength on the inflowing jet, and as such eliminates the potential for more complex behavior associated with the low-frequency variability and multiple dynamical regimes

observed in these jet–gyre systems (see McCalpin and Haidvogel 1996; Primeau 1998), a complicating feature we wished to eliminate from the system we studied.

We pose the eddy-mean flow interaction problem in terms of a time-mean state and the variability about this mean state. We spin the system up to steady state (domain-integrated enstrophy is nearly constant with time) and then accumulate turbulent statistics for a period long enough so that they are insensitive to the integration time. We use these statistics to diagnose dynamical quantities to gain insight into the dominant eddy-mean flow interaction mechanisms and also to quantify the changing eddy forcing when inflowing jet parameters are varied around GS- and KE-appropriate values. For full details, see the appendix.

It is worth mentioning that, although the model is highly simplified, there are several indications in past observations of the GS and in the recent analysis of new observations in the KE region (see Jayne et al. 2009; Waterman 2009) that give some confidence that both the simplifications that the idealized model employs and the physics that it retains are appropriate to these WBC jets. For example, observations in the deep ocean in the KE system indicate that the velocity structure below the thermocline has only a very weak depth dependence (Jayne et al. 2009). As such, a model with simplified vertical structure should suffice. Second, pointwise energy balances in the GS system indicate that both baroclinic and barotropic mechanisms are active (Dewar and Bane 1989). Observations of the KE also indicate the jet is likely subject to a mixed instability mechanism (Waterman 2009). As such, a model with the capacity to support both barotropic and baroclinic instability mechanisms is necessary. Finally, it is now widely appreciated that the GS is a highly time-dependent current, which exhibits fluctuations in speed comparable to its mean speed (Fofonoff 1981). There are several indications in KE observations that the KE system is similarly very nonlinear: perturbation velocities are on the order of the mean velocity, and observed wave phase speeds are on the order of (and often less than) individual particle speeds (Waterman 2009). As such, fully nonlinear dynamics are essential.

3. The barotropic case

We first examine the effect of eddies on the time-mean circulation in a typical WBC-scaled barotropic configuration. For reference, properties of the instantaneous and time-mean circulation for a typical barotropic case are shown in Fig. 2. The instantaneous circulation is characterized by large meanders, closed rings, and waves that are radiated from the barotropically unstable jet. As was found in Jayne et al. (1996), the time-mean circulation is characterized by a pair of counterrotating recirculation gyres that flank a time-mean zonal jet.

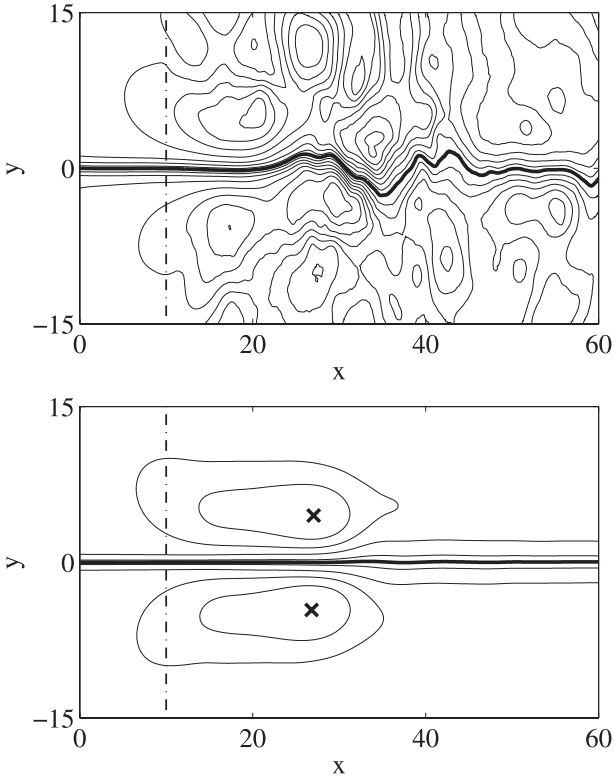

FIG. 2. A snapshot of the (top) instantaneous and (bottom) time-mean circulations (streamfunctions) for the typical barotropic case relevant to a WBC jet extension ($A = -1.0$, $l = 1.0$, and $\beta = 0.05$; see the appendix for parameter definitions). The dashed–dotted line at $x = 10$ (in this and relevant following figures) denotes the extent of the western sponge layer. In (bottom), × marks denote the locations of the maximum time-mean recirculation transport.

a. Insights from the eddy potential vorticity flux divergence

Following previous investigations exploring the role of eddies in driving recirculation gyres in WBC jet systems, we first examine the eddy forcing of the time-mean circulation through consideration of the eddy contribution to the time-mean Reynolds decomposed vorticity budget. Here, the effect of eddies appears as a forcing term given by the negative of the divergence of their PV flux, $-\nabla \cdot (\overline{\mathbf{u}'q'})$, and this satisfies the time-mean PV balance,

$$\overline{\mathbf{u}} \cdot \nabla \overline{q} = -\nabla \cdot (\overline{\mathbf{u}'q'}) \tag{1}$$

(note that we neglect the contribution of friction because it is negligible in the time-mean PV balance in the model interior). It was found to be most insightful to consider this forcing in a transformed Eulerian mean (TEM) framework (Andrews and McIntyre 1976, 1978). The transformation amounts to a repartitioning of mean and eddy

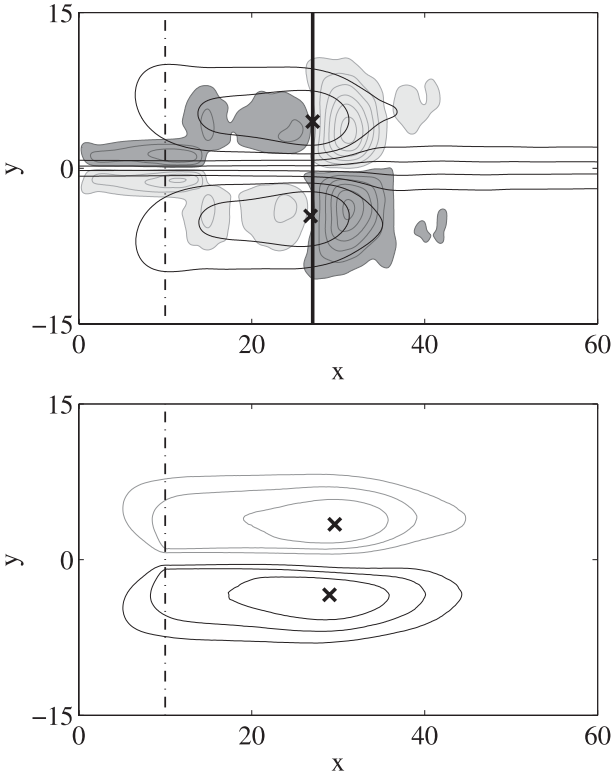

FIG. 3. (top) The eddy vorticity forcing given by the negative of the time-mean residual eddy vorticity flux divergence (filled contours) overlaid on properties of the time-mean streamfunction (black contours) for the typical barotropic case. Positive values of the eddy forcing (a residual eddy vorticity flux convergence) are shaded light gray and negative values (a residual eddy vorticity flux divergence) are shaded dark gray. The × marks denote the locations of the maximum time-mean recirculation transport. (bottom) The time-mean circulation driven by linear dynamics forced by the above eddy vorticity forcing field. Black contours indicate positive values of the eddy-driven streamfunction, whereas gray contours indicate negative values. The × marks denote the locations of the maximum time-mean eddy-driven transport.

fluxes so that the transformed eddy fluxes include only nonskew (divergent) components [those components of the eddy flux that are skew (i.e., directed normal to the mean gradient and thus advective in nature) are incorporated into the ''mean flux''; for a full discussion, see Plumb and Ferrari 2005]. In the case of the barotropic WBC jet, such a transformation results in removing the large cancelation between mean and eddy flux divergences and hence highlights the small residual eddy forcing that is significant in the dynamics.

This net ''eddy vorticity forcing'' is visualized in the top panel of Fig. 3. The time-mean circulation driven by this forcing, which is computed as that which satisfies Eq. (1) for the eddy vorticity forcing shown above, is shown in the bottom panel. Here, the direct responsibility of the eddies in driving the time-mean recirculation gyres is demonstrated.

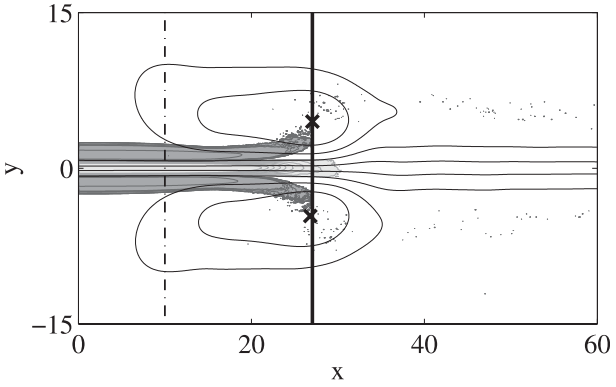

FIG. 4. The along-stream evolution of the meridional PV gradient of the time-mean jet $\partial\overline{q}/\partial y$ (filled contours) overlaid on properties of the time-mean streamfunction (black contours) for the typical barotropic case. Positive values of the time-mean meridional PV gradient are shaded light gray, and negative values are shaded dark gray. The × marks denote the locations of the maximum time-mean recirculation transport. The vertical black line indicates the boundary between the upstream and downstream regions: the along-stream location of the maximum time-mean recirculation transport and approximately where the time-mean jet is first necessarily stabilized to its barotropic instability.

Examining the pattern of the residual eddy vorticity flux divergence, we see that the net eddy forcing is dominated by a dipole pattern of eddy vorticity flux convergence (divergence) north (south) of the jet axis downstream of the along-stream location of maximum time-mean recirculation transport. Through the dominant time-mean PV balance between this eddy forcing and the rate of mean planetary vorticity advection, this drives mean meridional motions away from the jet and forces the flanking recirculations.

The picture of the net eddy forcing also shows a second important feature: a sharp transition from eddy forcing of one sign to that of the opposite sign across the along-stream location of the maximum time-mean recirculation transport on either flank of the jet. The correspondence suggests that the along-stream location of this switch in sign of the eddy forcing determines the along-stream location of maximum recirculation transport. Useful to the purpose of understanding the effect of eddies on the time-mean circulation and the mechanism that permits that effect, we note that this location is observed to also relate to a critical location in the along-stream evolution of the stability properties of the time-mean jet. In particular, it corresponds to approximately where the time-mean meridional PV gradient $\partial\overline{q}/\partial y$ on the flanks of the jet first ceases to be negative or more precisely where $\beta = \partial^2\overline{u}/\partial y^2$, where $\overline{u}$ is the time-mean zonal velocity, at the locations of the minima in the jet's time-mean meridional PV gradient profile. Importantly, it corresponds to where the time-mean jet profile first ceases to satisfy the

necessary condition for barotropic instability (Fig. 4). In short, the effect of the eddies on the time-mean circulation in this configuration is observed to undergo a fundamental change across the along-stream boundary between where the time-mean jet is unstable upstream and where it has been stabilized (by the effect of the eddies) downstream, which results in defining the along-stream location of maximum recirculation transport. We will now refer to these two regimes of eddy-mean flow interaction behavior as the ''upstream region'' and ''downstream region,'' respectively, noting that they are defined as upstream and downstream of the along-stream location where the time-mean recirculation transport is maximized and the time-mean jet is first necessarily stabilized.

b. *Insights from the eddy potential vorticity flux and its relation to the background potential vorticity gradient*

We explore the role of the stability properties of the time-mean jet in determining the eddy-mean flow interactions by considering the implications for the relation between the time-mean eddy PV flux and the background time-mean PV field $\overline{q}$. Here we find the picture to be significantly clarified by considering only the divergent part of the eddy PV flux (computed from a rotational and divergent decomposition of the full eddy PV flux diagnosed from the model; for details, see Jayne and Marotzke 2002). This, unlike the full eddy PV flux, which is dominated by a large rotational component, is predominantly across $\overline{q}$ contours and emphasizes two distinct regimes of behavior in the upstream and downstream regions.

The divergent part of the time-mean eddy PV flux is visualized in relation to the $\overline{q}$ field and its meridional gradient $\partial\overline{q}/\partial y$ (the most relevant component of the background PV gradient to consider given the dominant meridional orientation of the divergent eddy PV flux) in Fig. 5. The visualization demonstrates that the along-stream location of maximum recirculation transport and where the time-mean jet is first stabilized is also the along-stream location where the divergent part of the time-mean eddy PV flux switches its orientation from southward to northward. This, in combination with the background time-mean PV gradient implied by the unstable time-mean jet in the upstream region and the stabilized time-mean jet in the downstream region, then results in distinct patterns of upgradient and downgradient time-mean eddy PV fluxes. As a consequence, eddies play two distinct roles in feeding back on the time-mean circulation, with each effect localized to a distinct along-stream region.

First consider the upstream region. Here, eddies act to stabilize the jet through a downgradient PV flux inside the jet, which acts to destroy the mean PV gradient that is making the jet unstable. The downgradient eddy flux

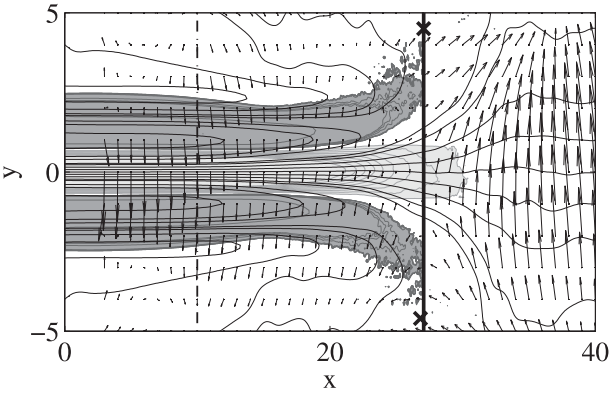

FIG. 5. A visualization of the time-mean eddy PV flux relative to the time-mean PV field and its meridional gradient for the typical barotropic case. Vectors indicate the divergent part of the time-mean eddy PV flux, black contours indicate the time-mean PV field $\overline{q}$, and the shading indicates the sign of the meridional gradient of the time-mean PV field $\partial\overline{q}/\partial y$ (with light gray indicating positive values of the time-mean meridional gradient and dark gray indicating negative values). The $\times$ marks denote the locations of maximum time-mean recirculation transport. The vertical solid line indicates the boundary between the upstream and downstream regions.

can be usefully thought of as a westward ''effective eddy force'' acting to decelerate the jet at its axis, as is seen in a visualization of the effect of eddies on the time-mean zonal momentum budget in the TEM framework, a forcing directly related to the divergent part of the PV flux (for details, see Plumb and Ferrari 2005) (Fig. 6). On the flanks of the jet, where the sign of the meridional PV gradient is opposite to that on the jet axis, the southward eddy PV flux is actually upgradient, but this also acts to stabilize the jet by providing an effective eastward force and accelerating the jet on its flanks, hence acting to further reduce the jet's large-scale horizontal shear.

In contrast, in the downstream region, the northward eddy PV flux in combination with a positive time-mean PV gradient everywhere implies that here the eddies act to drive time-mean flows through an upgradient PV flux localized just downstream of the upstream region–downstream region boundary. It is this upgradient flux that allows the eddies to accelerate time-mean flows and drive the time-mean recirculations, details of which are discussed further in the next section.

c. *Insights into the eddy-driving mechanism from enstrophy variance considerations*

To gain further insight into the mechanism that permits the eddies to flux PV up the mean PV gradient and drive the time-mean recirculations, we consider terms in the enstrophy variance budget.

Upgradient and downgradient eddy PV fluxes have implications for the enstrophy variance budget because eddy enstrophy generation, $-\overline{(\mathbf{u}'q')}\cdot\nabla\overline{q}$, is the product

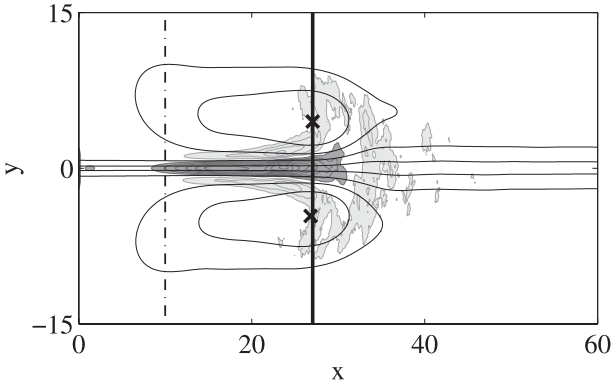

FIG. 6. The effect of eddies on the time-mean circulation as visualized by the zonal component of the effective eddy force in the TEM framework for the typical barotropic case. The zonal component of the effective eddy force $\{F_x = [\partial\overline{(u'u')}/\partial x] - \partial\epsilon/\partial x - [\partial\overline{(u'v')}/\partial y]$ where $\epsilon = (1/2)[\overline{(u'u')} + \overline{(v'v')}]\}$ (filled contours) overlaid on properties of the time-mean streamfunction (black contours). Positive values corresponding to an effective eastward eddy force are shaded light gray, and negative values corresponding to an effective westward eddy force are shaded dark gray. The × marks denote the locations of maximum time-mean recirculation transport. The vertical solid line indicates the boundary between upstream and downstream regions.

of the time-mean eddy flux of PV, $\overline{(\mathbf{u}'q')}$, and the time-mean PV gradient, $\overline{q}$, and, as such, is directly related to the sense of the eddy vorticity transport relative to the time-mean gradient. We visualize the negative of this quantity, in essence eddy enstrophy destruction $\overline{(\mathbf{u}'q')} \cdot \nabla\overline{q}$ (so positive values indicate regions of upgradient time-mean eddy PV fluxes) for the barotropic case in Fig. 7. Consistent with the picture of the eddy PV flux relative to the time-mean PV field and its gradient, Fig. 7 highlights the existence of two important regions of upgradient eddy fluxes permitting the eddy driving of time-mean flows: on the flanks of the time-mean jet upstream of jet stabilization (where eddies act to stabilize the jet by driving flows to broaden it) and just downstream of jet stabilization (where eddies act to drive the time-mean recirculations). As in the case of the eddy vorticity forcing, the importance of the region downstream of jet stabilization in the eddy driving of the recirculation gyres is highlighted. Investigation into the individual terms that contribute to the eddy enstrophy generation term $[\overline{u'q'}(\partial\overline{q}/\partial x)$ vs. $\overline{v'q'}(\partial\overline{q}/\partial y)]$ reveal that this pattern of along-stream evolution is sourced in the pattern of the along-stream evolution of the zonal gradient of the time-mean PV field, $\partial\overline{q}/\partial x$. In particular, upgradient fluxes downstream of jet stabilization result from the change from a four-lobed pattern of $\partial\overline{q}/\partial x$ associated with the along-stream evolution of a barotropically unstable jet profile, to a two-lobed pattern of $\partial\overline{q}/\partial x$ associated with the along-stream evolution of a barotropically stable jet profile (Fig. 7, bottom left). The observation further suggests that the fundamentally different effect of eddies on the time-mean circulation in the upstream versus downstream regions is a result of differences in the mean background PV gradient they act upon.

Insight into what allows this upgradient eddy PV flux in the downstream region comes from consideration of the other terms in the enstrophy variance budget. In the zonal-mean eddy-mean flow interaction problem (a much more commonly studied problem given its relevance to the atmosphere), the enstrophy variance budget (assuming eddy enstrophy advection, a triple correlation term, is small) reduces to a two-term balance between eddy enstrophy destruction and dissipation, $\overline{(\mathbf{u}'q')} \cdot \nabla\overline{q} = -D$, where D represents the dissipation of eddy enstrophy. This two-term balance guarantees that, given dissipation is always positive, eddy enstrophy destruction is negative and hence that the eddy PV flux is always down the mean gradient. This argument is the basis of downgradient turbulence closures. In the time-mean problem with zonal dependence however, time-mean convergences and divergences of the advection of eddy enstrophy, $\overline{\nabla \cdot \mathbf{u}(q'^2/2)}$, now also may play a role, providing an additional term to potentially balance the eddy enstrophy destruction term, and hence permit upgradient eddy PV fluxes [the time-mean enstrophy variance budget is now $\overline{(\mathbf{u}'q')} \cdot \nabla\overline{q} \sim -D - \overline{\nabla \cdot \mathbf{u}(q'^2/2)}$]. This additional term, the time-mean divergence of eddy enstrophy advection, for the WBC-typical barotropic jet is visualized in Fig. 8.

Consideration of the time-mean divergence of eddy enstrophy advection illustrates the important role that zonal variation and in particular the spatial separation of regions of eddy growth and decay resulting from the jet's zonal advection (a phenomenon that results in regions of significant time-mean eddy enstrophy flux divergence and convergence) plays in this problem. Consider first the regions of time-mean eddy enstrophy divergence in Fig. 8 found in the core of the jet and on the flanks of the jet in the upstream region. Here, eddy growth combined with the jet's advection produces a time-mean divergence of eddy enstrophy, which in the problem with zonal dependence acts in the same sense as dissipation and therefore requires a downgradient eddy PV flux to form a local balance. Farther downstream, however, that variance advected by the jet from the unstable region decays. This results in regions of time-mean eddy enstrophy convergence, including an important localized convergence just downstream of jet stabilization. This convergence is significant enough to overcome dissipation and allow upgradient eddy fluxes in this region as seen in Fig. 7. In short, it is the separation in space between regions of eddy enstrophy generation by the unstable jet and eddy enstrophy dissipation downstream of jet stabilization that is key. Advection of eddy enstrophy from the region of

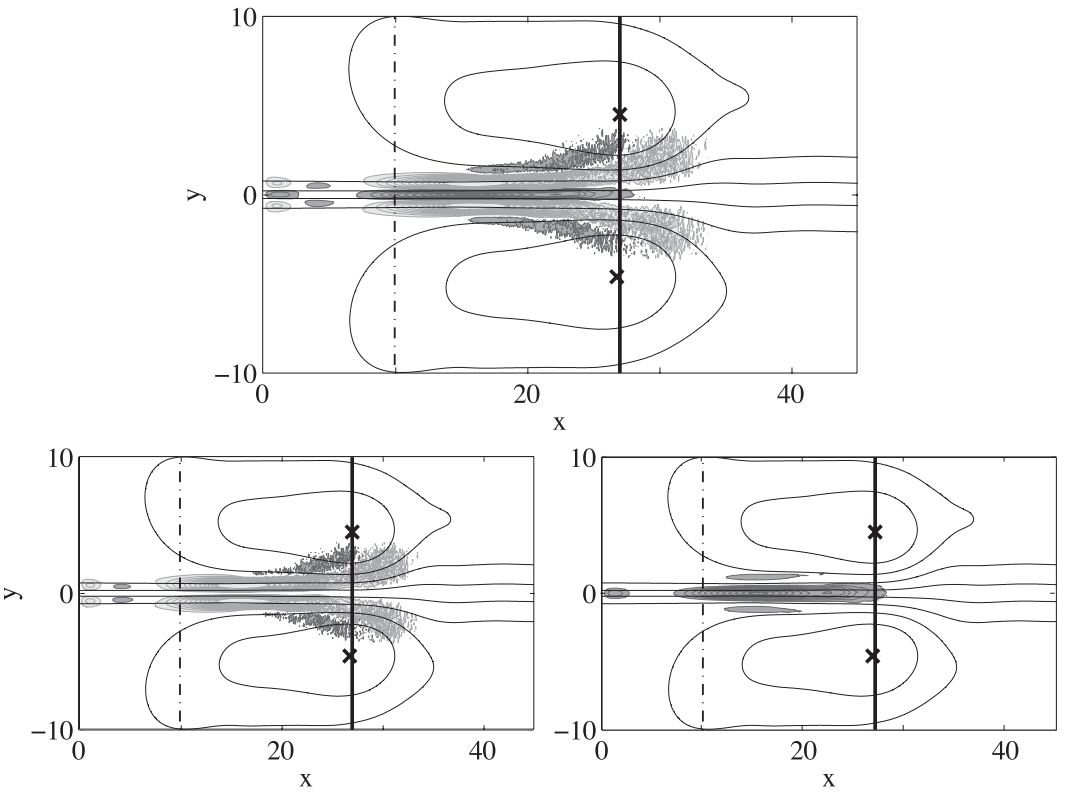

FIG. 7. (top) The negative of the time-mean eddy enstrophy generation term (eddy enstrophy destruction) (filled contours) overlaid on properties of the time-mean streamfunction (black contours) for the typical barotropic case. Positive values of eddy enstrophy destruction (indicating upgradient eddy PV fluxes) are shaded light gray and negative values (indicating downgradient eddy PV fluxes) are shaded dark gray. The relative contributions of the two terms making up the time-mean eddy enstrophy generation term: (bottom left) $\overline{u'q'}(\partial\overline{q}/\partial x)$ and (bottom right) $\overline{v'q'}(\partial\overline{q}/\partial y)$. The $\times$ marks denote the locations of maximum time-mean recirculation transport. The vertical solid line indicates the boundary between upstream and downstream regions.

eddy growth to the region of eddy decay results in an eddy enstrophy convergence that permits an upgradient eddy PV flux and ultimately the eddy-driving of the time-mean recirculation gyres.

d. A conceptual model of a localized wave radiator downstream of jet stabilization

The eddy vorticity forcing field (Fig. 3) shows the importance of the region downstream of jet stabilization to the eddy forcing of the time-mean circulation, whereas the time-mean eddy PV flux and the time-mean eddy enstrophy destruction field (Figs. 5, 7) implicate that it is here that eddies flux PV up the mean gradient and drive the time-mean recirculation gyres. A potentially useful model for understanding how eddies drive the mean flow in this downstream region is suggested by the similarity of the downstream region eddy vorticity forcing pattern to that of the simple model of a localized wavemaker on a β plane discussed first by Haidvogel and Rhines (1983) and more recently by Waterman and Jayne (2010, manuscript submitted to *J. Phys. Oceanogr.*). This conceptual model is potentially useful in understanding the eddy-driving mechanism because, as was shown in these studies, the fluxes associated with the waves or eddies generated by a localized wavemaker can drive time-mean recirculation gyres west of the forcing through the process of nonlinear eddy rectification.

This comparison between the eddy vorticity forcing field in the downstream region of the barotropic jet and in the localized wavemaker model is illustrated in the top panels of Fig. 9. The black circle in the latter denotes the region where a localized oscillatory vorticity forcing is applied. Specifically, this forcing is described by an oscillating source–sink of vorticity (with zero time-mean vorticity input) with an angular frequency on the order of $(2\pi/60)$ days^{-1} and a spatial distribution of the form of a Laplacian of a Gaussian (the black circle delineates the zero contour) with an amplitude equivalent to a wind stress per unit mass on the order of 0.1 m^{-1} s^{-2} or an Ekman pumping velocity on the order of 1×10^{-5} m s^{-1}

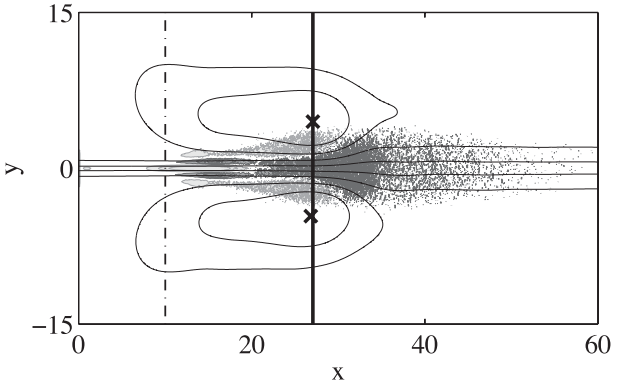

FIG. 8. The divergence of the time-mean advection of eddy enstrophy (filled contours) overlaid on properties of the time-mean streamfunction (black contours) for the typical barotropic case. Positive values (a divergence of eddy enstrophy advection) are shaded light gray, and negative values (a convergence of eddy enstrophy advection) are shaded dark gray.

(i.e., forcing parameters that are equivalent to typical oceanic synoptic scales). See Waterman and Jayne (2010, manuscript submitted to *J. Phys. Oceanogr.*) for further details. The comparison shows both eddy vorticity forcing fields are characterized by a dipole pattern consisting of a vorticity flux divergence in the southern half of the forced region and a vorticity flux convergence in the northern half of the forced region. The bottom panels of Fig. 9 illustrate the time-mean circulation that results from the above eddy vorticity forcing, computed as the solution to Eq. (1) forced statically by the eddy vorticity forcing field shown above. Consistently, both are characterized by a pair of counterrotating time-mean recirculation gyres west of the forcing.

Similarities between the dynamics of the region downstream of jet stabilization and the dynamics of the localized wavemaker are further seen in the energetics. If one examines the spatial distribution of eddy energy associated with the along-stream evolution of the time-mean jet (Fig. 10, top left), one sees that the growing instability of the jet in time followed by the subsequent dissipation of those eddies after the jet has been stabilized, when combined with jet's advection, results in a localized maximum of eddy kinetic energy located just downstream of jet stabilization. This ''bullet'' of eddy energy is not unlike the localized source of eddy activity generated by the localized wave maker (Fig. 10, top right), and the similarity makes the relation of the mechanism of recirculation driving in the jet and by the wavemaker seem plausible. Examination of the mean to eddy kinetic energy conversion rate in the jet in this region $\{\overline{u'^2}(\partial\overline{u}/\partial x) + \overline{u'v'}[(\partial\overline{u}/\partial y) + (\partial\overline{v}/\partial x)] + \overline{v'^2}(\partial\overline{v}/\partial y)$, where u and v are the zonal and meridional components of velocity and an overbar and prime denote a time-mean and eddy quantity, respectively} (Fig. 10, bottom left) also shows a small region of eddy to mean energy conversion that is similar to that inside the forced region of the wavemaker (Fig. 10, bottom right).

4. The baroclinic case

We next consider the eddy-mean flow interactions in the model in a baroclinic configuration more appropriate to an oceanic WBC jet. Properties of the instantaneous and time-mean circulation in each of the two layers are shown in Fig. 11. The instantaneous circulation in the upper layer is characterized by waves radiated from the upper-layer jet and intense upper-layer jet meandering downstream. In the lower layer, there are deep recirculations upstream and an intense eddy field downstream. Like the barotropic case, the time-mean circulation is dominated by time-mean recirculation gyres that flank the time-mean zonal jet. These recirculations exist in both layers and are weakly depth dependent.

a. The eddy effect on the mean circulation: Similarities and differences to the barotropic case

We perform an analogous diagnosis of the eddy effect on the time-mean circulation as in the barotropic case, noting that vorticity now includes both relative vorticity and thickness, the two-layer equivalent of buoyancy, contributions. The eddy vorticity forcing and the resulting eddy-driven circulation in each layer are shown in Fig. 12, and the divergent component of the time-mean eddy PV flux relative to the time-mean PV field and its meridional gradient in each layer is shown in Fig. 13. The along-stream evolution of the time-mean jet's stability properties, defined by a necessary condition for instability that requires the total meridional PV gradient to change sign in either the horizontal or the vertical, is evaluated by looking for changes of sign in the PV gradient both in horizontal maps of the layered PV gradients (Fig. 13) and in the vertical (Fig. 14). Finally, visualization of the eddy enstrophy generation and advection terms in the typical baroclinic configuration is given in Fig. 15.

From these collective diagnoses, we conclude that the general picture of the eddy effect on the time-mean circulation in the baroclinic, mixed instability case shares many important similarities to that in the barotropic configuration: eddies play two distinct roles acting to stabilize the jet to its large-scale shear (now both horizontal and vertical) and to drive the time-mean recirculations, and each effect is localized to a distinct along-stream region defined by the stability properties of the time-mean jet. Similar to the barotropic case, the eddy vorticity forcing (Fig. 12) is dominated by a dipole pattern of eddy vorticity flux convergence (divergence) north (south) of the jet

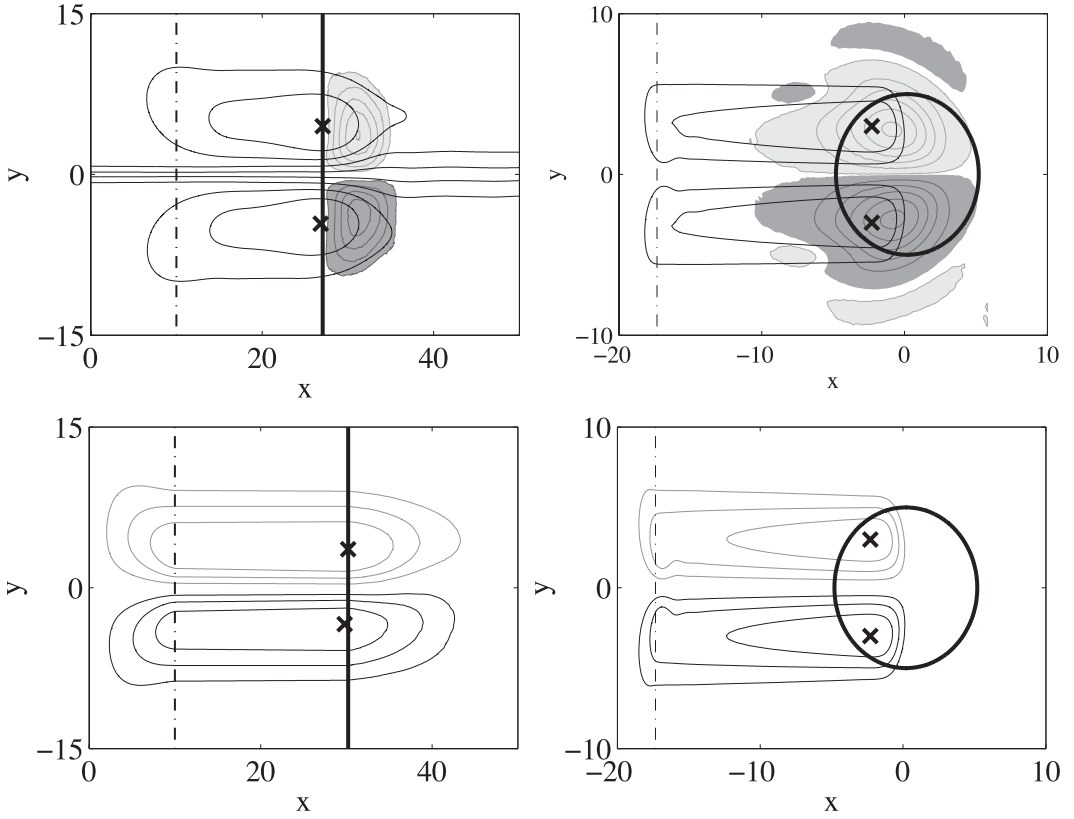

FIG. 9. (top left) The eddy vorticity forcing (filled contours) for the region downstream of jet stabilization in the typical barotropic case vs (top right) that for the wavemaker model. The black line in the former denotes the boundary between the upstream and downstream regions, and only forcing downstream of this boundary is applied. The circle in the latter denotes the region where a localized oscillatory vorticity forcing is applied. Black contours are of the time-mean streamfunction from the fully nonlinear solution. (bottom) The time-mean circulation that results from the above eddy vorticity forcing, computed as the solution to Eq. (1) forced by the above eddy vorticity forcing field. Black contours indicate positive values of the eddy-driven streamfunction, whereas gray contours indicate negative values.

downstream of the along-stream location of maximum time-mean recirculation transport in both layers. This is understood to be responsible for the driving of the recirculations and suggests that the eddy driving in this two-layer case may remain essentially barotropic and share similar mechanics to the barotropic case. Examination of the along-stream evolution of the horizontal and vertical structure of the system's time-mean vorticity gradient field (Figs. 13, 14) shows again a clear relation between the along-stream location of maximum recirculation transport, the switch in sign of the eddy forcing, and the time-mean jet's stability properties. Here, the relevant stability criterion that defines this location is whether the time-mean vorticity gradients in each layer change sign in the vertical, because this is the instability criterion that remains satisfied for the longest along-stream distance. Finally, visualization of the eddy enstrophy generation and advection terms in the typical baroclinic configuration (Fig. 15) suggests that, from the point of view of enstrophy, a similar mechanism to the barotropic case operates in the mixed instability case, at least in the upper layer. Here, the picture of eddy enstrophy destruction and advection is characterized by a pattern of time-mean eddy enstrophy generation and destruction associated with the along-stream evolution of a barotropically unstable jet in the upstream region and a concentration of upgradient eddy PV flux collocated with significant eddy enstrophy convergence in the downstream region.

There are, however, some important differences between the barotropic and baroclinic configurations that arise because of key differences in the background time-mean PV gradient and its along-stream evolution in the mixed instability case where both horizontal and vertical shears contribute. These make the dynamics in the upstream "unstable jet" regime fundamentally baroclinic and quite different from the dynamics in the barotropic configuration. These differences are perhaps best seen in an examination of the divergent component of the time-mean eddy PV flux relative to the time-mean PV field and its meridional gradient, shown in each layer in Fig. 13. Here is

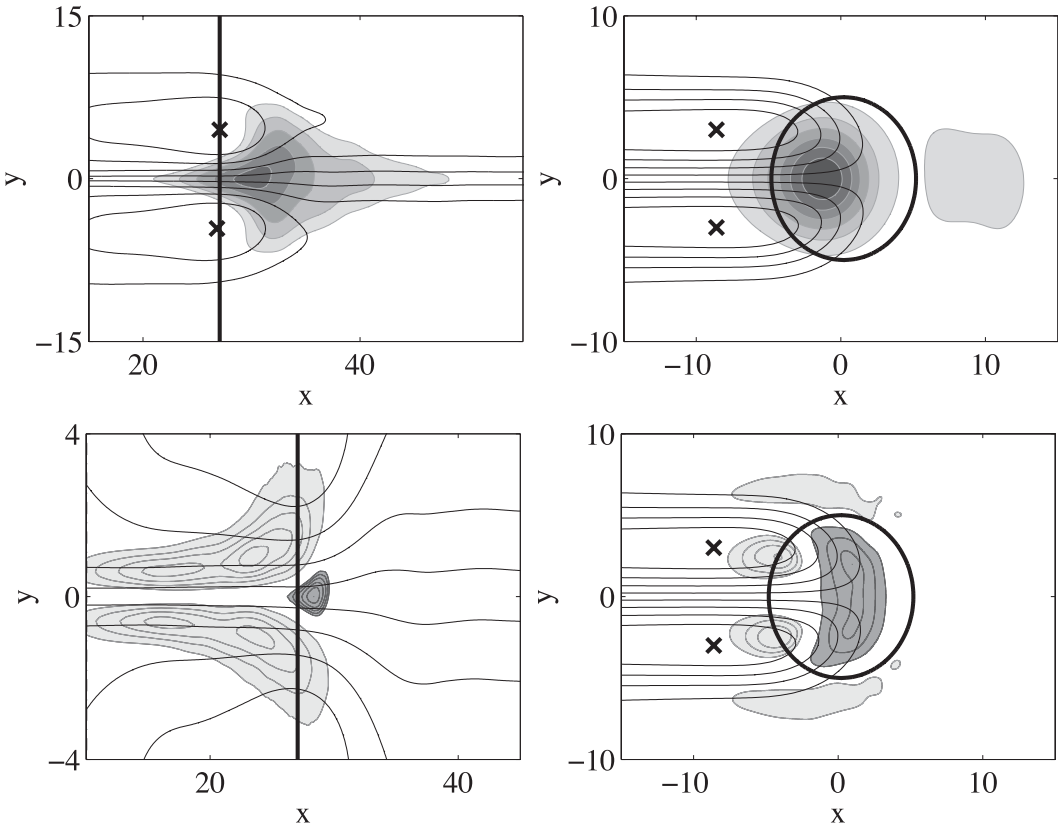

FIG. 10. A comparison of (left) the downstream region of the jet and (right) the localized wavemaker model in terms of energetics as visualized by (top) the time-mean variance of the streamfunction $\overline{\psi'\psi'}$ and (bottom) the mean to EKE conversion rate, which is defined in the text.

illustrated the important difference that, in the baroclinic case, the switch in sign of the divergent time-mean eddy PV flux occurs not at the along-stream location of maximum recirculation transport and jet stabilization as in the barotropic case but instead upstream, where the contribution of the horizontal shear of the upper-layer jet giving rise to the three-lobed pattern of the time-mean meridional PV gradient in the upper layer, $\partial\overline{q}_1/\partial y$, ceases to dominate the upper-layer time-mean PV gradient. As it will be seen, it is useful to consider this boundary as dividing the upstream unstable jet region in the baroclinic case further into two along-stream regions: a western zone of the upstream unstable jet region where the time-mean eddy PV flux is southward and horizontal shear of the upper-layer jet dominates $\partial\overline{q}_1/\partial y$ ($0 < x < \sim 16$ in the typical baroclinic case) and an eastern zone of the upstream unstable jet region where the time-mean eddy PV flux is northward and vertical shear dominates $\partial\overline{q}_1/\partial y$. The secondary local maximum in recirculation strength upstream of the system's unstable–stable boundary ($x \sim 18$ in the typical baroclinic case) is one manifestation of the fact that a two-regime description of the mixed instability jet's upstream unstable region is appropriate. As outlined below, the additional structure to the along-stream description of the eddy-mean flow interactions in the upstream region of the mixed instability case has important implications.

Considering first these implications for the upper layer, we note first that the southward eddy PV flux in the western zone of the upstream region is, as in the barotropic case, downgradient inside the jet and upgradient on the jet flanks and as such acts to stabilize the upper-layer jet to its horizontal shear. However, the northward eddy PV flux in the eastern zone of the upstream region is instead upgradient, resulting in a time-mean convergence (divergence) north (south) of the jet just upstream of the maximum in time-mean recirculation transport and the unstable–stable jet boundary. This is the opposite pattern to the barotropic case at this equivalent location in the jet's along-stream evolution. As such, here eddies contribute to, as opposed to acting against, the recirculations driven by the eddy fluxes in the downstream region. This less effective ''internal'' closure by the upstream region in the upper layer is manifested in the fact that more of the recirculations close in the western boundary sponge layer compared to the barotropic case. It is significant because it implies that recirculations driven by downstream dynamics in the baroclinic

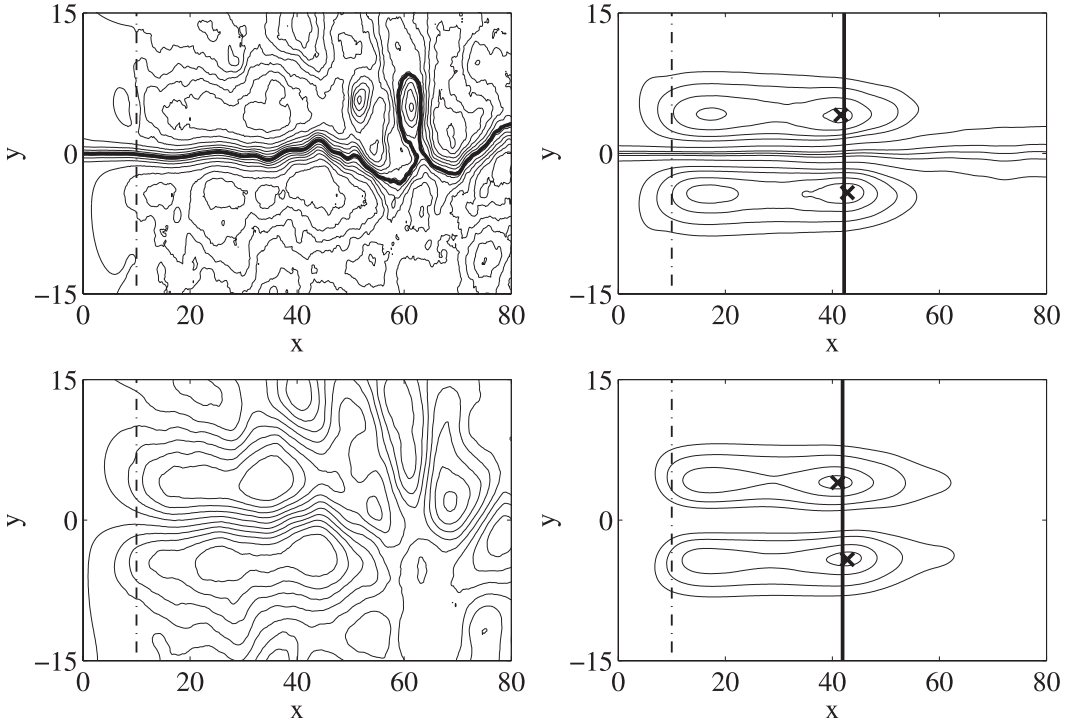

FIG. 11. As in Fig. 2, but for the typical baroclinic case relevant to a WBC jet extension ($A = -1.0$, $l = 1.0$, $\beta = 0.03$, $S_1 = 1.0$, and $S_2 = 0.25$). Shown are the (top) upper and (bottom) lower layers.

case can more easily extend their influence westward until an opposing outside force (such as frictional effects in the western boundary layer) act to close the recirculations. In this way, the recirculation-driving mechanism in the baroclinic configuration is more effective at driving recirculations that extend broadly beyond the localized vicinity of the eddy forcing that generated them.

Turning our attention to the lower layer, we see a similar picture where the dynamics in the upstream unstable region are again best described as being made up of two along-stream regimes. In the western zone of the upstream region, where the upper-layer dynamics is dominated by the upper-layer jet's horizontal shear, the southward eddy PV flux is upgradient at the jet axis and, as such, acts to accelerate a lower-layer jet. In this way, the eddies also act to stabilize the system to its vertical shear. In the eastern zone of the upstream region, where vertical shear of the system dominates, the northward eddy PV flux is still downgradient in the lower layer and, as such, like the barotropic case, produces a pattern of vorticity flux divergence (convergence) north (south) of the jet axis just upstream of the maximum in recirculation strength familiar from our analysis of the barotropic configuration. Hence, here lower-layer eddies, like in the barotropic case, are responsible for a partial interior closure of the recirculation gyres driven by dynamics in the downstream wave-radiator region.

b. *The roles and relative importance of relative vorticity versus thickness vorticity fluxes*

As mentioned previously, the addition of baroclinic dynamics results in two available mechanisms by which eddy fluxes can influence the dynamics: namely, relative vorticity fluxes as in the barotropic case and thickness or stretching fluxes of PV, the layered equivalent of buoyancy fluxes. Of interest are the roles and relative importance of each in the baroclinic configuration. To gain insight, we decompose the eddy forcing into its relative vorticity and thickness components and ask what roles each play and what is their relative importance in a GS- or KE-like parameter regime.[3] This decomposition is shown in Fig. 16. The exercise allows us to see that, in this parameter regime, the eddy relative flux divergence dominates the eddy vorticity forcing (approximately by an order of magnitude) in both layers and acts in a very similar way as in the barotropic case (with the caveat of the important difference of

[3] We note that the sponge layer on the western boundary may have a significant influence on the partition of the eddy vorticity flux between relative vorticity and thickness components in an analogous way to how no-slip and partial-slip boundary conditions on the western wall seem to control whether relative vorticity or thickness eddy fluxes maintain the upper-ocean recirculations in double-gyre models (see Berloff et al. 2007). How the sponge layer controls the role of these fluxes is at this time unknown.

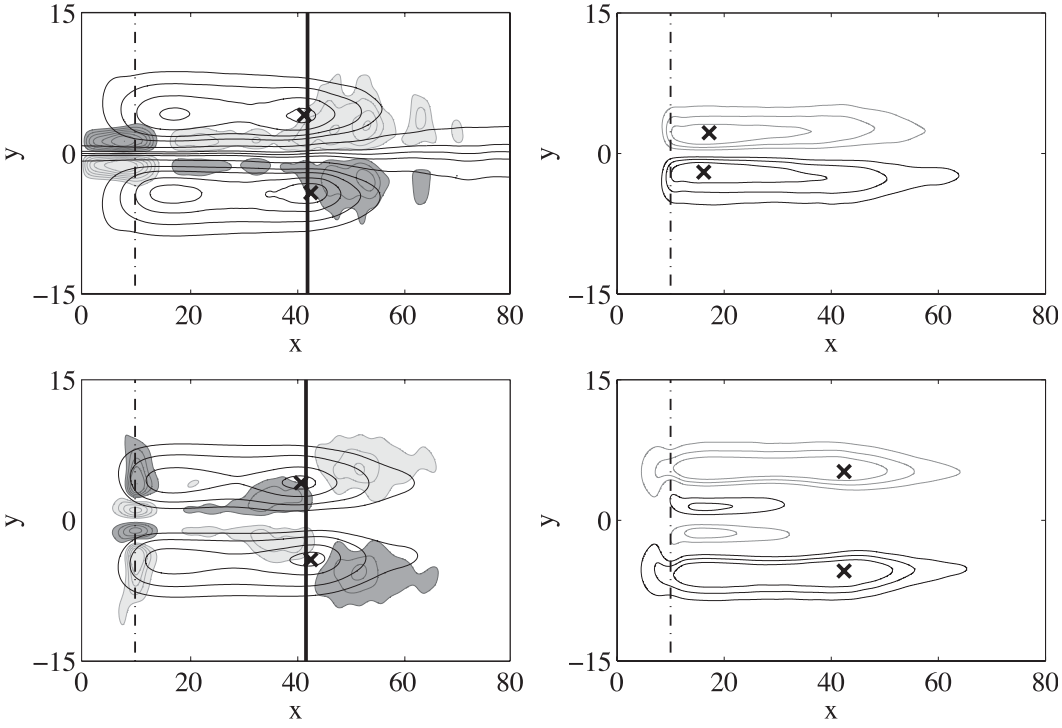

FIG. 12. As in Fig. 3, but for the typical baroclinic case. Shown are (left) the eddy vorticity forcing and (right) the corresponding eddy-driven streamfunction for the (top) upper and (bottom) lower layers.

the existence of an upgradient eddy PV flux in the eastern zone of the upstream region in the upper layer). This further suggests that the mechanism responsible for the eddy driving of the recirculations in this two-layer case remains essentially a barotropic one. In this respect, the addition of baroclinicity does not seem to significantly alter the eddy-driving mechanism.

Examining the role of thickness fluxes in more detail reveals the role that they play in driving the lower-layer recirculations and making the recirculations more barotropic. As can be seen in Fig. 17, thickness fluxes contribute to the eddy forcing by adding a dipole of vorticity flux convergence and divergence at the along-stream location of maximum time-mean recirculation transport. In the lower layer, this is in the same sense as the eddy relative vorticity forcing (i.e., in the sense generated by an upgradient eddy PV flux) and, as such, drives a pair of recirculations that enhance the lower-layer recirculation strength. In contrast, in the upper layer, the thickness flux forcing pattern opposes the relative vorticity flux forcing pattern (i.e., it is in the sense of a downgradient eddy PV flux) and, as such, drives a pair of counterrotating recirculation gyres that act to make the upper-layer recirculations weaker. In this way, the thickness fluxes in the baroclinic configuration act to make the eddy-driven recirculations more barotropic than they would be in the absence of these fluxes.

5. Dependence on system parameters

A second goal of this study was to understand how the eddy effect on time-mean state properties depends on system parameters, and to examine this we performed a series of studies that varied parameters around GS- and KE-like values. In the case of the barotropic jet, the variation of interest was the degree of barotropic instability of the inflowing jet, achieved via the variation of the nondimensional β parameter, $\beta = \beta_{\mathrm{dim}} L^2/U$, where β_{dim} is the meridional gradient of the planetary vorticity and L and U are typical length and velocity scales of the flow. Decreasing this parameter can be thought of as equivalent to making the jet stronger and/or sharper, hence having greater horizontal shear and being more barotropically unstable. In the baroclinic case, we again vary the nondimensional β parameter, which in this case can be thought of as equivalent to varying the upper-layer jet strength, influencing both the horizontal shear in the upper layer and the vertical shear between layers.

Results of these parameter studies are summarized in Figs. 18 and 19, dimensionalized by scales appropriate to the KE. They are viewed as a function of the net (inflow–outflow) PV anomaly associated with the imposed inflowing and outflowing jet profiles, because this is the relevant forcing amplitude of the interior eddy PV flux divergence. Here, it is seen that the properties of the time-mean

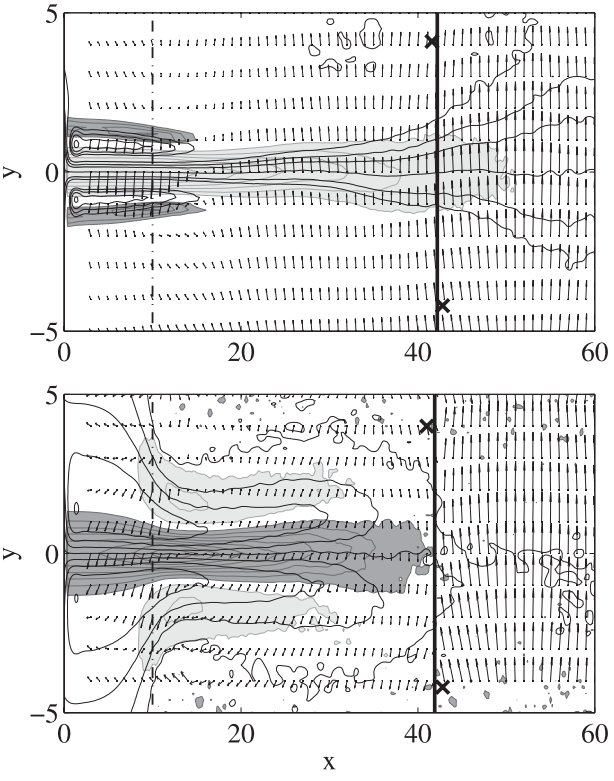

FIG. 13. As in Fig. 5, for the typical baroclinic case. Shown are the (top) upper and (bottom) lower layers.

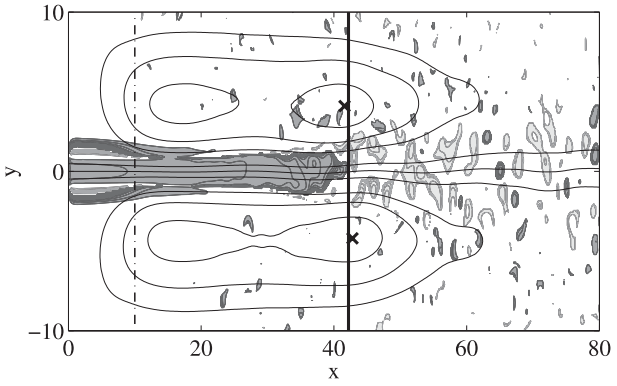

FIG. 14. The along-stream evolution of the ratio of the time-mean meridional PV gradient in the upper layer to that in the lower layer, $(\partial\overline{q}_1/\partial y)/(\partial\overline{q}_2/\partial y)$ (filled contours), for the typical baroclinic case. This is the relevant change of sign to define the two-layer jet's stability properties because this is the instability criterion that remains satisfied for the longest along-stream distance. Positive values are shaded light gray, and negative values are shaded dark gray. Black contours indicate properties of the time-mean barotropic streamfunction $(\overline{\psi}_1 + \overline{\psi}_2)$.

circulation, in particular of the time-mean recirculations (their strength and their meridional and zonal extent), are sensitive to the net PV anomaly of the inflowing jet that is the source of the eddy variability that drives them. In particular, in both the barotropic and baroclinic cases, as the inflowing WBC jet becomes more unstable, the recirculations tend to shrink in their zonal extent while expanding in their meridional extent (Figs. 18, 19, right). Recirculation strength also is strongly dependent on the net inflowing PV anomaly, generally increasing with inflowing jet supercriticality (Figs. 18, 19, left). In both the barotropic and baroclinic cases, the increase in barotropic recirculation strength with PV anomaly is rapid for small values of PV forcing amplitude. For larger forcing amplitudes, however, a different regime of dependence is observed: in the barotropic case, the rapid quadratic dependence slows to a linear dependence, whereas, in the baroclinic case, the barotropic recirculation strength changes from rapidly increasing with PV forcing amplitude to decreasing with PV forcing amplitude. We label the two regimes of behavior observed in each case as ''weakly nonlinear'' and ''strongly nonlinear,'' with the transition between them defined empirically by the forcing amplitude that marks this observed change in the dependence of mean recirculation strength on the PV forcing amplitude. We feel this distinction is significant to recognize, because the behavior observed in the barotropic case in the weakly nonlinear regime is consistent with the prediction of a quadratic dependence of the eddy-driven mean flow strength on forcing amplitude from weakly nonlinear theory applied to the wavemaker configuration (for details, see Waterman and Jayne 2010, manuscript submitted to *J. Phys. Oceanogr.*). The dynamics responsible for the change in mean-flow strength dependence observed in the strongly nonlinear regime remains of interest and is currently under investigation.

In attempts to better understand the observed dependence of recirculation extent on the supercriticality of the inflowing jet, we consider the parameter study results in the context of linear stability calculations. With the shrinking of the zonal extent of the recirculations as the inflowing jet is made more supercritical, the along-stream location of maximum time-mean recirculation transport (and jet stabilization) moves upstream. The dependence of this key along-stream location on forcing amplitude is shown explicitly in the left panels of Fig. 20. Here, it is seen that, for weakly unstable jets, the along-stream location of maximum time-mean recirculation transport is located far along stream. This location, however, moves rapidly upstream as jet supercriticality is increased, until saturation is achieved. Partial insight into this dependence is suggested by the results of the linear stability calculation for the inflowing jet profiles considered and specifically the result that the inverse growth rate shows a very similar dependence, decreasing as the jet profile becomes more unstable (Fig. 20, right). The correspondence of these results is encouraging and suggests that the linear stability

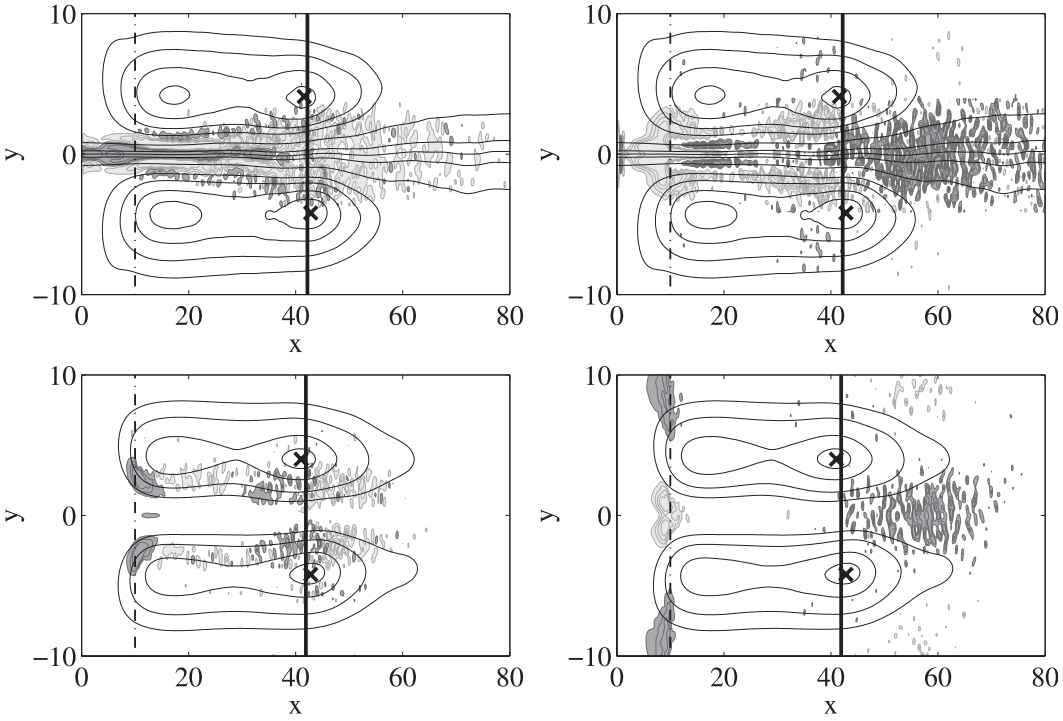

FIG. 15. (left) The time-mean eddy enstrophy destruction and (right) time-mean eddy enstrophy advection divergence (filled contours) for the typical baroclinic case for (top) the upper layer and (bottom) the lower layer. Positive values (i.e., eddy enstrophy generation and divergence) are shaded light gray, and negative values (i.e., eddy enstrophy destruction and convergence) are shaded dark gray.

calculation predictions for the properties of the fastest growing mode have some utility in predicting the properties of the fully nonlinear solution, and it further supports the claim that weakly nonlinear dynamics have validity in a WBC-appropriate parameter regime. The similarity in the behavior of these two quantities leads to the hypothesis that the along-stream location of maximum recirculation transport (and jet stabilization) is related to the distance the jet advects the growing instability in the time it takes for the eddies to grow to sufficient size such that their fluxes are effective at stabilizing the time-mean jet profile. The growth rate is faster for more unstable jets, but the magnitude of the PV anomaly associated with these jets is also larger, so distance to stabilization is not a linear function of inverse growth rate alone. Comparing barotropic and baroclinic cases, it can be seen that in the baroclinic case the along-stream location of mean jet stabilization and maximum recirculation transport tends to be farther downstream for an equivalent forcing amplitude, whereas the inverse growth rate tends to be shorter. This suggests that the eddies must grow to larger amplitude in the baroclinic case compared to the barotropic one for their fluxes to be capable of stabilizing the time-mean jet profile, a consequence perhaps of the fact that they must stabilize the jet both to its horizontal and vertical shear in the mixed instability case. As for the change in the length scale of the recirculations downstream of the location of maximum recirculation transport and jet stabilization, which is also observed to shrink dramatically as the supercriticality of the inflowing jet is increased, the explanation for this apparent increase in the rate of eddy decay remains under investigation. Key to the explanation may be the changing eddy wavenumbers selected by the changing instability and the consequent changing ability of the eddies to ''swim'' upstream against the jet because of their zonal group velocity's dependence on wavenumber. The applicability of this hypothesis is currently under investigation.

6. Summary and discussion

A study of an idealized model of a WBC jet in a configuration and parameter regime relevant to the GS and KE systems has resulted in an expanded picture of eddy-mean flow interactions in WBC systems, in particular with respect to our understanding of how eddies act to both stabilize the WBC jet and drive the flanking time-mean recirculations. Like previous investigators (see, e.g., Hogg 1993, and references therein), we demonstrate the eddies, through the time-mean divergence of the eddy PV flux,

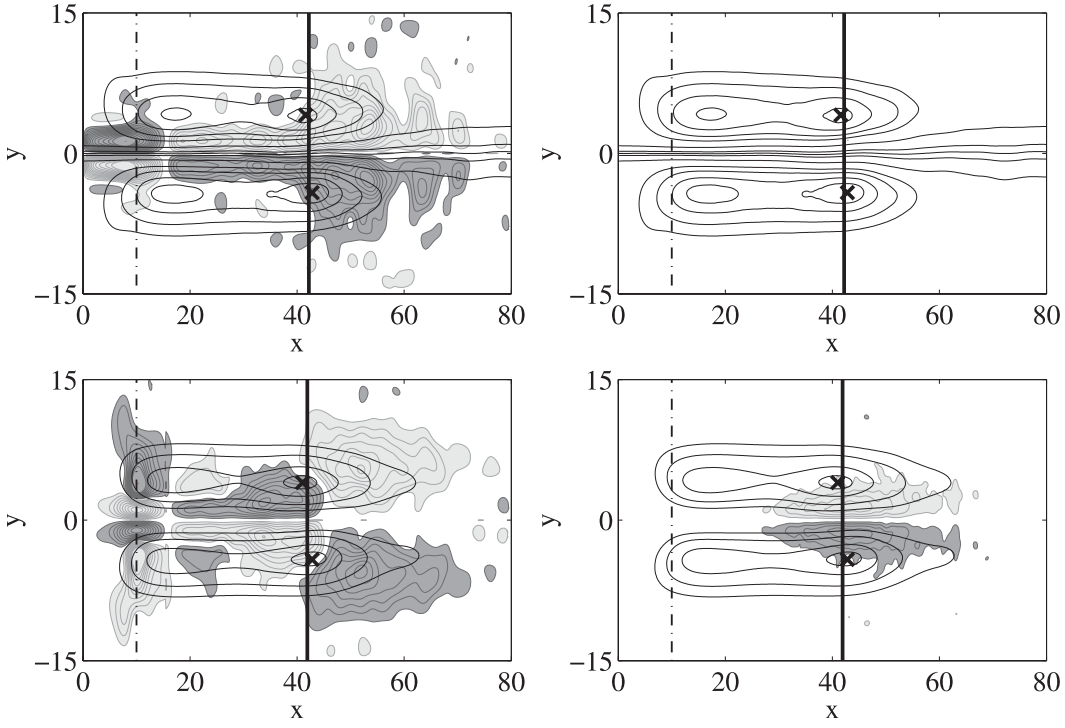

FIG. 16. The relative contributions of the (left) relative vorticity and (right) thickness flux components of the eddy vorticity forcing (filled contours) for the (top) upper and (bottom) lower layers. Contour intervals in each layer are common for relative and thickness contributions to determine their relative importance.

are capable of driving the time-mean recirculation gyres. This study furthers our understanding of the eddy-driving mechanism and the other roles that eddies play in this system by the following:

- It illustrates that eddies play two distinct roles in their feedback on the time-mean circulation in this configuration: 1) stabilizing the jet to its instability and 2) driving the time-mean recirculation gyres. It also localizes each effect to a distinct along-stream region defined by the stability properties of the time-mean jet. Upstream of jet stabilization, eddies act to stabilize the jet through downgradient fluxes of PV. Downstream of where the time-mean jet has (through the effect of the eddies) been stabilized, eddies act to drive the time-mean recirculations through the mechanism of an upgradient PV flux. Hence, zonal dependence in our description of the eddy effect is fundamental: the role of the eddies changes upstream versus downstream of where the WBC jet is stabilized.
- It argues for the importance of the stability of the time-mean jet in the eddy feedback effect because of its role in setting the structure of the background PV gradient the eddy fluxes act upon. The time-mean PV gradient is important in determining the spatial structure of where the time-mean eddy fluxes are upgradient versus downgradient, which impacts the pattern of time-mean eddy vorticity flux divergence and ultimately the eddy feedback effect. As will be discussed, the use of the time-averaged distribution of the PV gradient to evaluate the stability of the jet and the nature of the eddy-mean flow interaction cannot be justified on first principles; however, our model suggests that the time-mean distribution of the PV gradient does play an important role in the diagnosis of the eddy-mean flow interactions in this configuration (at least when defined in a framework of the time-mean state and the deviation from the time-mean state). It is as a consequence of this role that the along-stream location of the stabilization of the time-mean jet acts as a point of transition for many important drivers and indicators of the eddy feedback effect.
- It demonstrates that the upgradient eddy PV fluxes responsible for the driving of the recirculation gyres are permitted by a significant time-mean eddy enstrophy convergence in the downstream region that results from the generation of eddy enstrophy in the unstable jet regime, the advection of that eddy activity along-stream by the mean jet, and the dissipation of that eddy enstrophy downstream of jet stabilization. Here again, we see that zonal dependence is critical to the mechanism that permits the

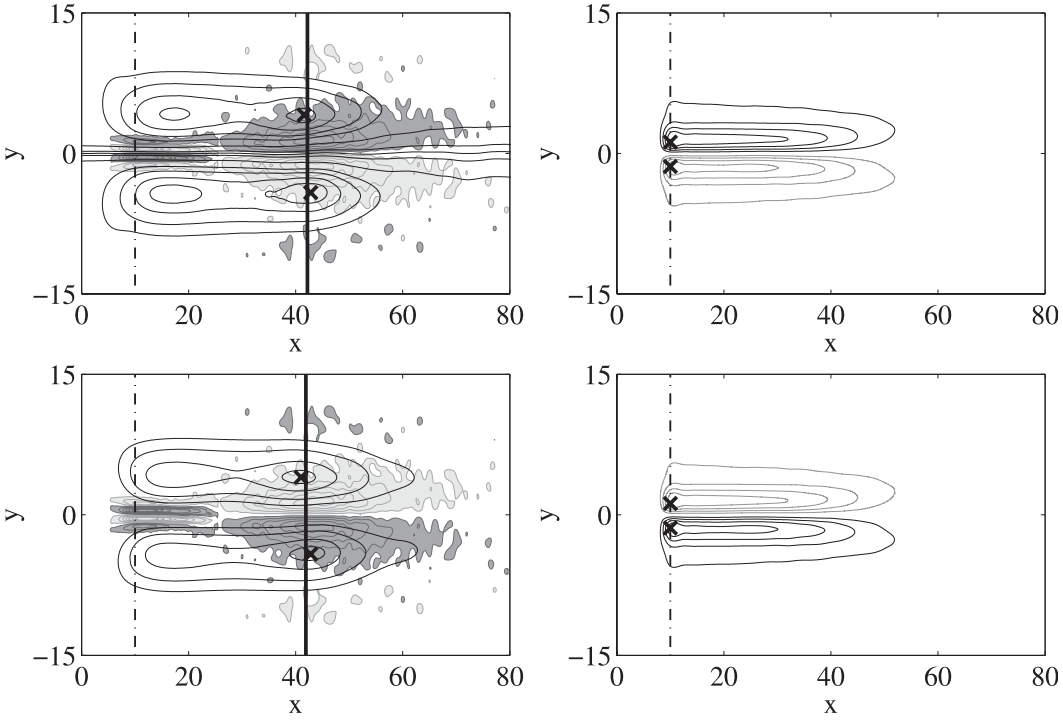

FIG. 17. (left) The eddy vorticity forcing resulting from the eddy flux divergence of thickness fluxes only and (right) the time-mean circulation it drives for (top) the upper and (bottom) lower layers. Black contours indicate positive values of the eddy-driven time-mean streamfunction, and gray contours indicate negative values.

eddies to drive the time-mean recirculations in this configuration.

- It provides a potentially useful model for the eddy driving of the recirculations in the downstream region: a localized wavemaker on a β plane. The time-mean recirculations can be understood as the result of the action of a localized source of eddy activity generated by the unstable jet stabilizing itself as the instability is advected downstream, acting on a PV gradient that is, in essence, just a modified β plane, given that the now stabilized time-mean jet no longer causes a reversal of sign in the time-mean meridional PV gradient. Potentially, the eddy-driving effect in the downstream region of WBC jet systems could be parameterized in this way.
- It highlights important similarities and differences in the eddy-mean flow feedback in the barotropic case versus the more oceanically relevant baroclinic mixed instability configuration. Like the barotropic case, the role of eddies in the along-stream evolution of the time-mean circulation in the baroclinic case continues to be usefully characterized as dividing into two along-stream regions. In the upstream region, the time-mean jet is unstable, eddy energy is growing, eddy enstrophy is being generated and advected away, and eddies act to stabilize the jet by fluxing PV downgradient and driving mean flows that reduce the system's horizontal and vertical shears. In the downstream region, the time-mean jet is stable, eddy energy is decaying, eddy enstrophy from the jet's advection is converging, and eddies act to drive the time-mean recirculations via a localized upgradient PV flux. In contrast to the barotropic case, additional structure to the eddy-mean flow interactions in the upstream region is generated as a consequence of additional structure in the along-stream evolution of the background time-mean PV gradient associated with the mixed instability. This has some significant consequences for the time-mean recirculations driven by the eddies, particularly in the upper layer, where the eddy-driving mechanism becomes more effective at driving recirculations that extend more widely beyond the localized vicinity of the eddy forcing that generated them. The dominance of eddy relative vorticity fluxes over eddy thickness fluxes suggests that, in the baroclinic case, the eddy-driving mechanism remains essentially a barotropic mechanism. Thickness fluxes act in the sense to drive lower-layer recirculations and make the recirculations more barotropic.
- It demonstrates that the properties of the eddy-driven time-mean recirculations are strongly dependent on the stability properties of the jet that generated them. This has significant implications if, for example, we wish to predict changes we might expect

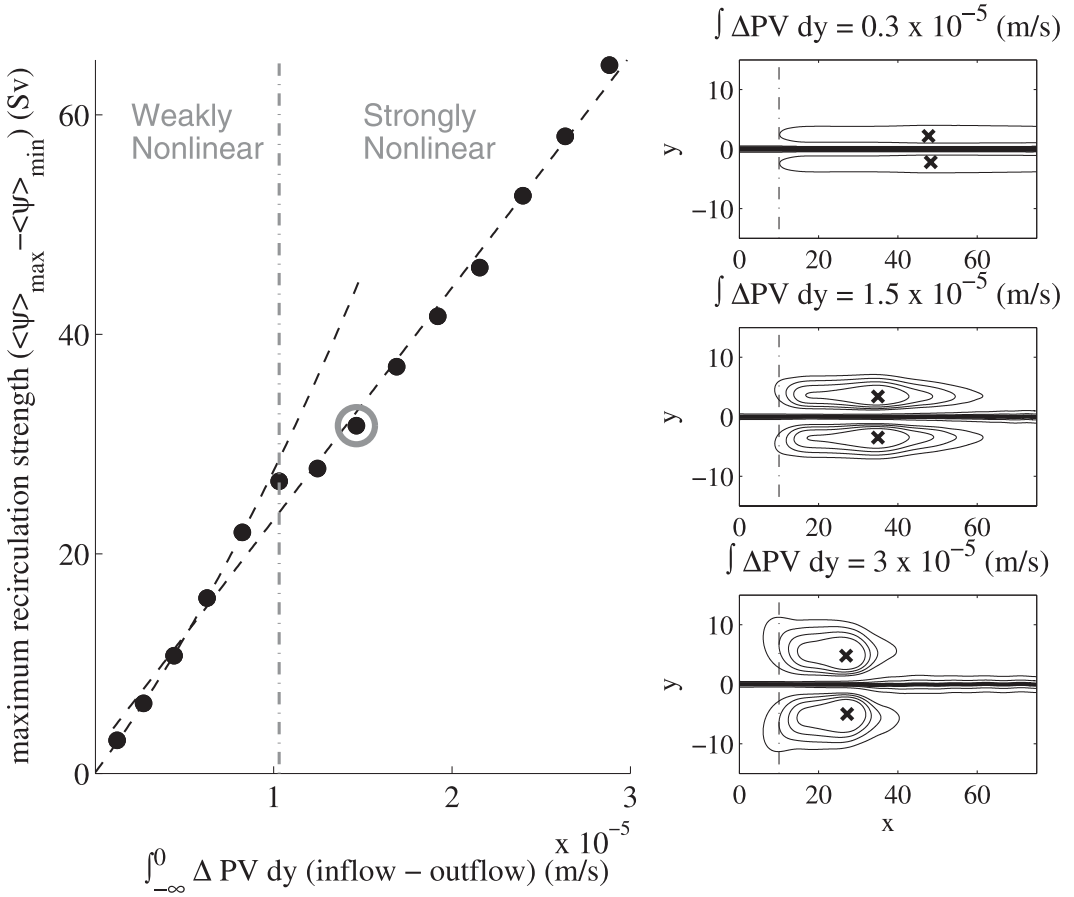

FIG. 18. (left) The dependence of time-mean recirculation strength (as measured by the maximum time-mean recirculation transport, $\overline{\psi}_{max} - \overline{\psi}_{min}$) on the PV forcing amplitude supplied by the inflowing unstable jet in a physically relevant range of parameters. The dashed vertical line indicates a transition from a weakly nonlinear to strongly nonlinear regime based on the observed change in the mean flow response from quadratic to linear in the forcing amplitude. An estimate for the supercriticality of the KE, determined from the synoptic mean velocity profile of the Kuroshio jet at the point of separation from the coast derived from satellite altimetry data (see Fig. 1), is indicated by the gray circle. (right) The time-mean circulation (streamfunctions) for (top) small, (middle) moderate, and (bottom) large inflowing jet supercriticalities showing the changing nature of the time-mean recirculation gyres as the entering jet becomes increasingly unstable.

to see in WBC jet transport and/or recirculation structure if oceanic conditions changed in such a way as to alter the stability properties of the WBC jet at the coast.

One of the major results of this study is that the nature of the eddy-mean flow interactions in the idealized WBC jet system studied is critically dependent on zonal position relative to the along-stream evolving stability properties of the time-mean jet. As alluded to above, despite its heuristic value in this case, it is important to recognize that the use of the time-averaged distribution of the PV gradient to evaluate the stability of the jet and the nature of the eddy-mean flow interactions cannot be justified on first principles (as formally stability involves the instantaneous flow and the spatial pattern of the perturbation field). Some other related caveats that should be made include the following:

- Although the temporal interpretation of the results seem to have heuristic value in explaining the observed eddy-mean flow interaction behavior, the relevance of spatial instabilities (i.e., disturbances with real frequency and complex zonal wavenumber corresponding to a system forced in a local region at constant frequency) also needs to be recognized. In papers on the temporal instabilities of the GS, for instance, many authors (e.g., Johns 1988; Xue 1991) agree that spatial instability is probably more relevant than the temporal variant in this application.

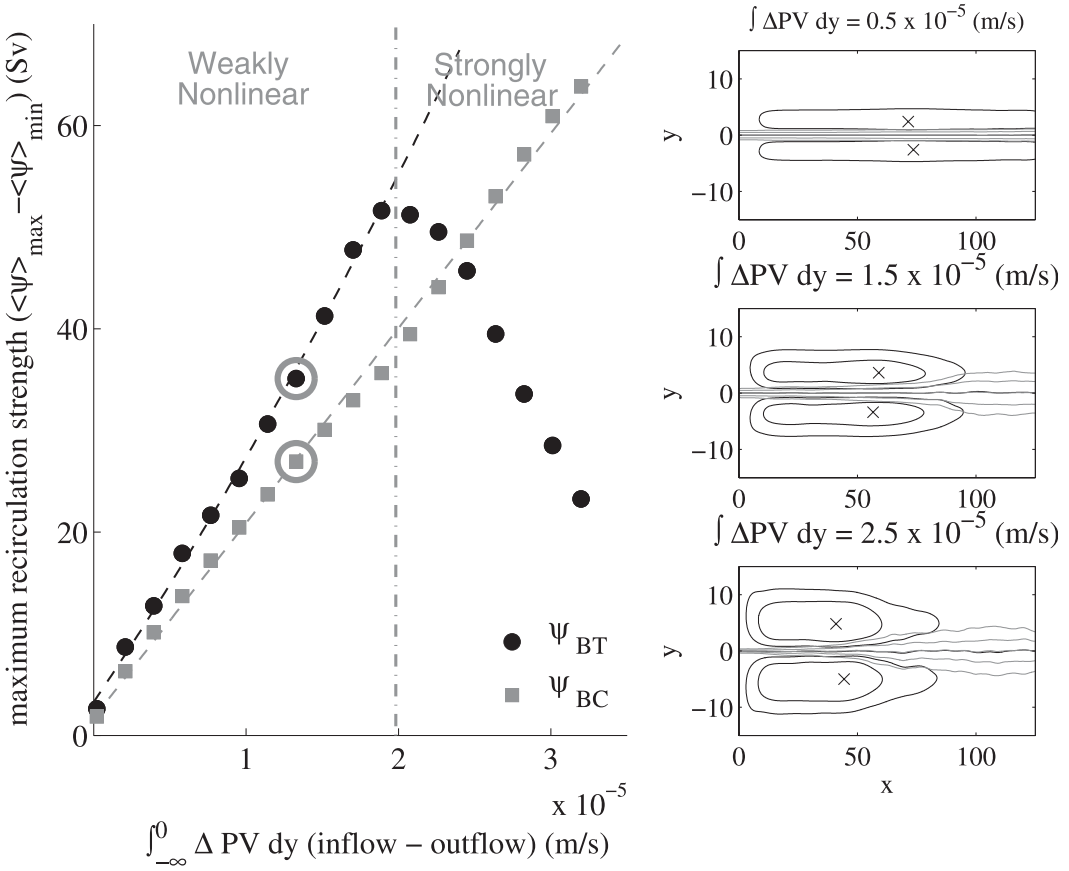

FIG. 19. As in Fig. 18, but for the baroclinic case. The barotropic recirculation strength ($\psi_{BT} = \psi_1 + \psi_2$) is shown by circles, and the baroclinic recirculation strength ($\psi_{BC} = \psi_1 - \psi_2$) is shown by squares. (right) Contours of the time-mean streamfunction show the barotropic circulation in black and the baroclinic circulation in gray.

- In addition to normal mode instabilities (both temporal and spatial), the relevance of pulse instabilities (i.e., the linear solution that represents the asymptotic solution to the evolution of a localized disturbance, as an approximation to the full initial value problem as time goes to infinity) should be considered. In particular, convective instabilities, a category of pulse instabilities where the disturbance ''propagates'' along the system as it grows in time, may be especially appropriate. If a system is convectively unstable and forced continuously with constant frequency at a local region, spatial instability is likely to occur. This scenario likely has relevance to the problem considered here.
- There is no local relation between ''local'' stability characteristics (based on local cross-sectional profiles) and the disturbance intensity or its interaction with the mean in currents whose cross-stream structure varies in the along-stream direction. Also, in cases where the advective time scale of the current is much less than the dissipation time, as in WBC jets, disturbances may propagate from unstable regions into stable regions and continue to extract energy from the mean and grow in amplitude (for a full discussion, see Pedlosky 1976). In general, the relation between the along-stream locations where the time-mean jet is first stabilized to its temporal instability, the instantaneous jet is first stabilized to its temporal instability, the jet is first stabilized to its spatial instability, EKE is maximized, and the recirculation strength is maximized needs to be examined more carefully.
- An understanding of time dependence in the along-stream location of instantaneous jet stabilization and how this relates to the nature of time-mean eddy-mean flow interactions is still required. The utility of our understanding of the long-period oscillation that exists in the finite-amplitude state of a baroclinic wave or packet of waves as discussed in Pedlosky (1970, 1972), as well as how this may translate to along-stream variation in the jet's stabilization point, also needs to be assessed. An evaluation of a time series of the model jet's behavior, which is currently underway, will hopefully provide some insight into these matters.

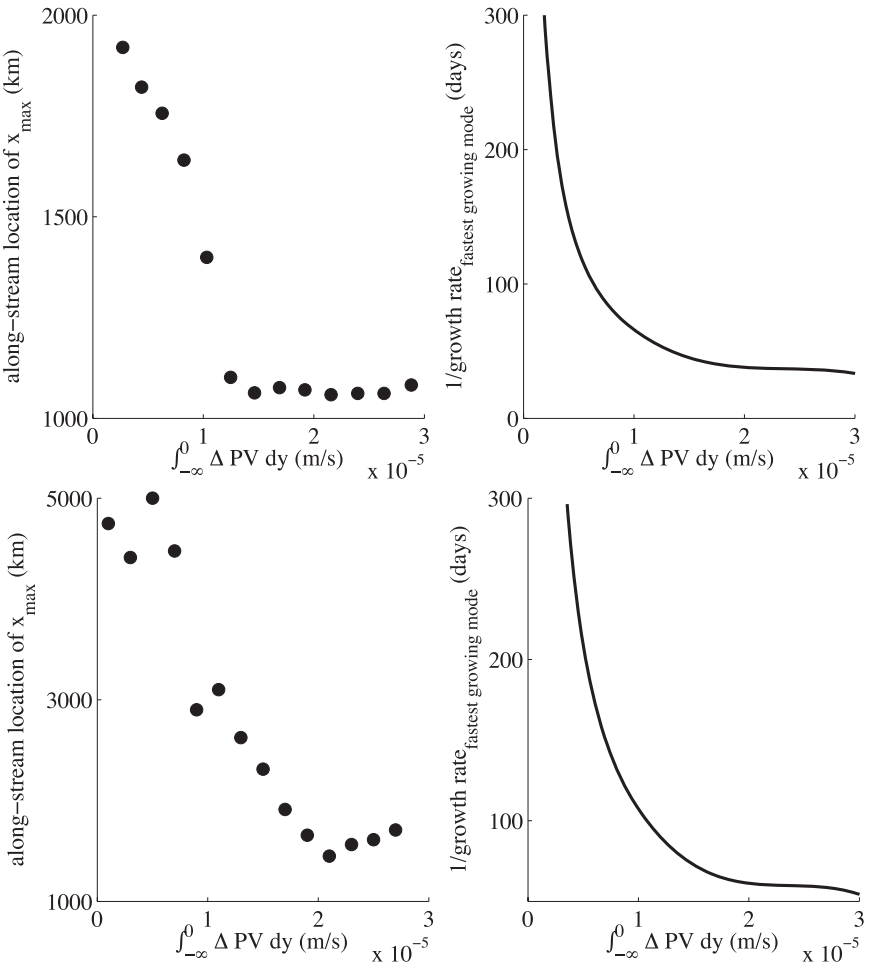

FIG. 20. The dependence of (left) recirculation zonal extent (as measured by the along-stream location of maximum time-mean recirculation transport, $\overline{\psi}_{\max} - \overline{\psi}_{\min}$) vs (right) the inverse growth rate (from the linear stability calculation for the inflowing jet profile) on forcing amplitude for the (top) barotropic and (bottom) baroclinic cases.

- Finally, as remarked on by one insightful reviewer, there exists a valid alternative interpretation of the dynamics at play that does not depend on the time-mean PV gradient and the stability properties of the time-mean jet as the interpretation presented here does. This is one that views the eddy-mean flow interaction dynamics as a consequence of a downstream source of eddies, generated by the large-amplitude meanders that develop in the jet at the along-stream location where the eddies grow to sufficient amplitude. These eddies are then responsible for time-mean fluxes of PV up the mean gradient which, via the wavemaker mechanism discussed, act to drive the inertial recirculations. In this description, downgradient eddy PV fluxes in the upstream region may also be due to eddies generated in the downstream region, if eddies found in the upstream region are those that are capable of "swimming" upstream against the jet from their downstream source. If valid, in this way, the system can develop a systematic distribution of eddy shape characteristics that results from the downstream source of eddies combined with shape-dependent eddy propagation characteristics. The eddy feedback effect is then, in part, a consequence of this spatial distribution of eddy shape properties. It is likely that both interpretations have a role to play and that the complete eddy effect is determined by the combined effects of the time-mean eddy vorticity flux divergence forcing that results from the along-stream evolving stability properties of the time-mean jet, as we have described here, in combination with the time-mean eddy vorticity flux divergence forcing that results from the along-stream evolving properties of eddy shape and propagation that result from the existence of a downstream wavemaker. Work on the role

of eddy shape and propagation characteristics in setting the eddy-mean flow interactions in this configuration is currently underway.

Ideally, the relevance of these theoretical results would be tested by looking for consistencies between model signatures and ocean observations. Unfortunately, because of the challenge of obtaining enough observational data to accurately calculate various eddy statistics, diagnostic studies of the relation between the mean or low-frequency state and eddies using direct observations have been rare. Some attempts have been made with limited data on regional scales, which provide tidbits for comparison, however, and many of these provide partial pictures of WBC jet dynamics that are consistent with the model dynamics observed. For example, current meter records analyzed by Dewar and Bane (1989) in the GS system at 73°W (250 km downstream of Cape Hatteras in what should be the upstream ''unstable jet regime'' if defined relative to the along-stream evolution of EKE) provide evidence of GS eddies acting to accelerate flows at abyssal levels while decelerating the mean jet at thermocline depths, consistent with the picture of the eddy forcing seen in the upstream unstable jet regime in the baroclinic model. Further, they provide observational evidence of a changing role of eddy effects in the along-stream evolution of the GS jet system consistent with the dynamics discussed here. By compiling various data sources at 73° and 68°W, these same authors conclude that the eddy field at 73°W, upstream of the EKE maximum (Reverdin et al. 2003), is significantly different in its effects on the GS than at 68°W (near the EKE maximum), transitioning from a state dominated by baroclinic instability upstream to barotropic instability near the along-stream location of maximum EKE. This evolution is also in agreement with the along-stream development of the WBC-representative mixed instability case. Finally, with respect to eddy vorticity forcing, measurements in the abyssal GS suggest that the eddy relative vorticity and thickness fluxes are of comparable strength there, with the eddy relative flux divergence being of the right sign and order of magnitude to drive a recirculation of the observed strength, whereas the thickness flux acts to make the recirculation more barotropic (Hogg 1993). Although relative vorticity fluxes dominate in the idealized WBC model studies here, the roles of the relative vorticity and thickness fluxes observed are consistent with model behavior.

Acknowledgments. The authors would like to gratefully acknowledge useful discussion with Joseph Pedlosky, Pavel Berloff, Glenn Flierl, Nelson Hogg, and John Whitehead. SW was supported by the MIT Presidential Fellowship and the National Science Foundation under Grants OCE-0220161 and OCE-0825550. The financial assistance of the Houghton Fund, the MIT Student Assistance Fund, and WHOI Academic Programs is also gratefully acknowledged. SRJ was supported by the National Science Foundation under Grants OCE-0220161 and OCE-0849808.

APPENDIX

The Numerical Model

a. Model equations

The numerical model used is the one described in Jayne and Hogg (1999) and modified to include two-layer dynamics. It is quasigeostrophic, on a midlatitude β plane, with linear bottom friction.

For barotropic runs, the model solves the fully nonlinear, barotropic quasigeostrophic potential vorticity equation (QGPVE) in nondimensional form,

$$\frac{\partial q}{\partial t} + J(\psi, q) = -R\nabla^2\psi, \tag{A1}$$

where q, the barotropic potential vorticity, is given by

$$q = \nabla^2\psi + \beta y. \tag{A2}$$

Here, ψ is the nondimensional streamfunction; R is a nondimensional bottom friction coefficient; and β is the nondimensional β parameter, $\beta = \beta_{\text{dim}}L^2/U$, where β_{dim} is the meridional gradient of planetary vorticity and L and U are characteristic length and velocity scales, respectively (taken to be the inflowing jet's width and magnitude). Hence, β represents the ratio of the scales of the horizontal gradient in relative vorticity associated with the inflowing jet to that of the horizontal gradient in planetary vorticity.

In the two-layer configuration, the model solves the Burger-number-weighted barotropic and baroclinic equations formed from the layered version of the QGPVE [$(1/S_2) \times$ layer 1 + $(1/S_2) \times$ layer 2 and layer 1 − layer 2, respectively], with bottom friction acting on the lower-layer vorticity. The barotropic vorticity prognostic equation is

$$\frac{\partial\left(\frac{1}{S_2}q_1 + \frac{1}{S_1}q_2\right)}{\partial t} + \frac{1}{S_2}J(\psi_1, q_1) + \frac{1}{S_1}J(\psi_2, q_2) = -\frac{1}{S_1}R\nabla^2\psi_2, \tag{A3}$$

and the baroclinic vorticity prognostic equation is

$$\frac{\partial(q_1 - q_2)}{\partial t} + J(\psi_1, q_1) - J(\psi_2, q_2) + \left(\frac{1}{S_1} + \frac{1}{S_2}\right) J(\psi_1, \psi_2) = R\nabla^2\psi_2, \quad \text{(A4)}$$

with

$$q_n = \nabla^2\psi_n + \beta y \mp \frac{1}{S_n}(\psi_1 - \psi_2) \quad n = 1, 2. \quad \text{(A5)}$$

Here, ψ_n is the nondimensional streamfunction in the nth layer, and S_n is the nth-layer Burger number, $S_n = [(ND_n/fL)]^2$, where N is the buoyancy frequency, D_n is the nth-layer depth, and f is the Coriolis frequency. Hence, S_n represents the ratio of the Rossby radius of deformation to the jet width in each layer, and the relative importance of stratification in the vertical to rotation in the horizontal.

The model is forced by the prescription of an unstable zonal jet inflow at the western boundary. For the cases presented here, the streamfunction at $x = 0$ in the upper layer is prescribed in the form of an error function,

$$\psi_1(x = 0, y) = A \operatorname{erf}\left(\frac{\ell}{y}\right), \quad \text{(A6)}$$

producing a Gaussian jet in zonal velocity with amplitude $(2/\sqrt{\pi})A$ and half-width ℓ. An inflow can also be prescribed in the lower layer, but, given our intentions to model the WBC jet entering the open ocean from the coast, no flow was prescribed at the western boundary in the lower layer for all cases discussed here.

As discussed in the text, the mass injected into the domain by the inflowing jet must be removed from the domain at the eastern boundary, and it is important to the relevance of the model to the along-stream development of a WBC jet in the open ocean that the eastern boundary condition does not control the upstream dynamics that we study. Hence, the robustness of our results were tested for varying zonal domain sizes and outflow conditions including a broad outflow constant in y, a broad stable outflowing jet, and an outflowing jet profile in a state of marginal barotropic instability {i.e., with a width given by $\ell = [(-8Ae^{-1.5})/(\beta\sqrt{\pi})]^{-1/3}$}. Results of these tests demonstrate that the upstream results we report on here are insensitive to the zonal domain extent and outflow condition provided: 1) the outflowing jet is ''less unstable'' than the inflowing jet (i.e., the outflowing PV anomaly is less than the inflowing PV anomaly); 2) the zonal extent of the domain is long enough to allow the inflowing unstable jet to stabilize well upstream of the eastern sponge layer; 3) the outflow condition removes mass from the domain at the same rate that the inflowing jet supplies mass to the domain; and 4) the eastern sponge layer is wide enough and/or friction in the eastern sponge layer is strong enough to allow the frictional contribution to the time-mean PV budget inside the sponge layer to force the jet profile in the eastern sponge to conform to the outflow profile at the eastern boundary.

b. Numerical method

Details on the numerical method can be found in Jayne and Hogg (1999). In the baroclinic case, the time rate of change of the barotropic and baroclinic vorticity is computed from the layer streamfunction and vorticity fields and then, after solving for the barotropic and baroclinic streamfunctions from the vorticity fields, the layer streamfunctions are computed and stepped in time using a third-order Adams–Bashforth scheme (Durran 1991). Integration in time and space is done using a scheme that is center differenced in the two spatial dimensions (an ''Arakawa A grid'') and advective terms are handled using the vorticity conserving scheme of Arakawa (1966). At each time step, the relative vorticity is inverted to find the streamfunction using the generalized Buneman algorithm (Adams et al. 1988).

The nondimensional grid spacing is 0.1 nondimensional length units (ndlu), and the number of grid points is 2501 (east–west) by 1501 (north–south). With the origin at the western boundary and the meridional center of the domain, this puts the eastern boundary at $x = 150$ and the northern boundary at $y = 75$ ndlu. Dissipative sponge layers, 10 ndlu wide at the western boundary and 20 ndlu wide at all other boundaries, absorb waves leaving the domain. The width of these sponge layers was chosen to be sufficient to eliminate basin modes from the domain, and the size of the domain was chosen to be sufficient such that interior dynamics we study are qualitatively insensitive to the northern, southern, and eastern sponge layers' extent and damping rate. The model configuration, putting the interior region we study in the context of the full model domain and the configuration of the sponge layers, is shown in Fig. A1.

The model is integrated for 15 000 nondimensional time units (ndtu) with a time step of 0.04 ndtu. Spinup to steady state is rapid in the barotropic case and slower in the baroclinic case (see Fig. A2). Results presented here are from runs integrated for 15 000 ndtu with turbulent statistics accumulated for the final 5000 ndtu (after both systems have reached steady state defined as domain-integrated enstrophy constant with time) and are qualitatively unchanged for longer periods of turbulent statistic accumulation.

c. Model parameters

We fix the nondimensional forcing parameters A (the jet strength) and ℓ (the jet width) ($|A| = \ell = 1.0$). Inflowing

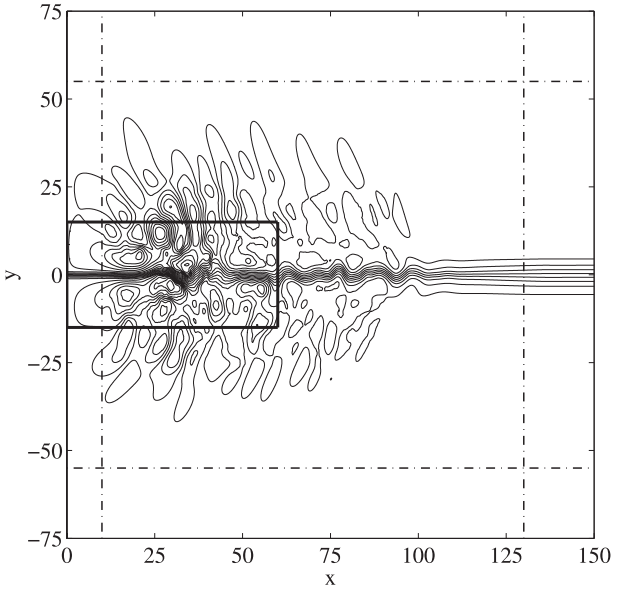

FIG. A1. The model configuration. A snapshot of the instantaneous streamfunction for the typical barotropic case as in Fig. 2, but showing the full model domain. Dashed–dotted lines denote the extent of the lateral sponge layers. The thick black box shows the interior region studied.

jet properties are then set by the value of nondimensional β, which can be thought of as setting the relative size of the horizontal shear of the WBC jet and hence its supercriticality to barotropic instability. The WBC-typical runs discussed have a value of β of 0.05, which results in a dimensional scaling of $L = 40$ km and $U = 1$ m s^{-1} [taking $\beta_{\text{dim}} = 2 \times 10^{-11}$ (m s)$^{-1}$] to make the inflowing jet profile consistent with the velocity and length scales of the Kuroshio jet where it separates from the coast (Fig. 1). Parameter studies discussed vary β in the range from 0.4 to 0.04 (barotropic case) and from 0.6 to 0.02 (two-layer case), which correspond to (taking the scale of the jet width to be fixed) a dimensional inflowing jet strength U in the range of ~0.1 to ~1 m s^{-1} (barotropic case) and in the range of ~0.01 to ~1 m s^{-1} (two-layer case). For reference, the GS has a value of nondimensional β in the range of 0.02–0.13 (Flierl et al. 1987).

In the case of the 2-layer runs, upper- and lower-layer Burger numbers need also to be specified. In all cases, a value of S_1 of 1.0 and S_2 of 4.0 are used, corresponding to a thermocline depth of approximately ~800 m in a ~5000-m-depth ocean, again typical of KE and GS scales. The nature of the stability explored is almost certainly dependent on the values of these parameters, although this is not explored in this work.

Away from the sponge layers the explicit friction, $R = 1 \times 10^{-6}$ (nondimensional), is chosen to be as low as possible consistent with numerical stability (dimensional values for the dissipation time scale range from ~10 to ~100 yr for the range of β values considered). Note that this makes the frictional contribution to the time-mean vorticity balance in the interior negligible relative to the other terms.

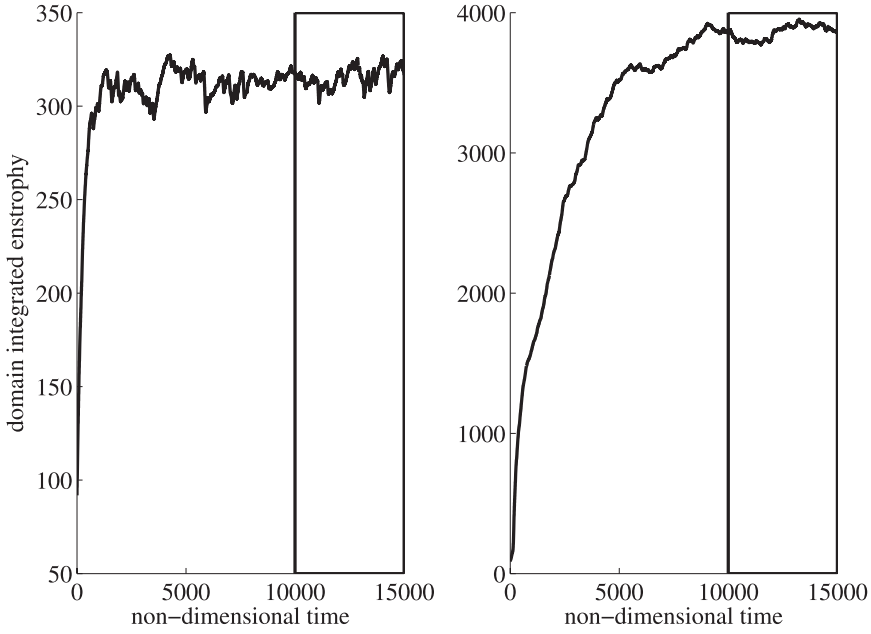

FIG. A2. Model spinup and turbulent statistics accumulation. The domain-integrated enstrophy as a function of integration time for the typical (left) barotropic and (right) baroclinic cases. In each case, turbulent statistics are accumulated for the final 5000 nondimensional time units, highlighted by the thick black boxes.

REFERENCES

Adams, J., P. Swartztrauber, and R. Sweet, 1988: FISHPAK: A package of FORTRAN subprograms for the solution of separable elliptic partial differential equations. Version 3.2.

Andrews, D. G., and M. E. McIntyre, 1976: Planetary waves in horizontal and vertical shear: The generalized Eliassen-Palm relation and the mean zonal acceleration. *J. Atmos. Sci.,* **33,** 2031–2048.

——, and ——, 1978: Generalized Eliassen-Palm and Charney-Drazin theorems for waves on axisymmetric mean flows in incompressible atmospheres. *J. Atmos. Sci.,* **35,** 175–185.

Arakawa, A., 1966: Computational design for long-term numerical integration of the equations of fluid motion: Part I: Two-dimensional incompressible flow. *J. Comput. Phys.,* **1,** 119–145.

Beliakova, N., 1998: Generation and maintenance of recirculations by Gulf Stream instabilities. Ph.D. thesis, Massachusetts Institute of Technology and Woods Hole Oceanographic Institution Joint Program, 224 pp.

Berloff, P., 2005: On the rectification of randomly forced flows. *J. Mar. Res.,* **63,** 497–527.

——, and S. Meacham, 1998: The dynamics of a simple baroclinic model of the wind-driven circulation. *J. Phys. Oceanogr.,* **28,** 361–388.

——, and J. McWilliams, 1999: Quasi-geostrophic dynamics of the western boundary current. *J. Phys. Oceanogr.,* **29,** 2607–2634.

——, S. Kravtsov, W. Dewar, and J. McWilliams, 2007: Ocean eddy dynamics in a coupled ocean–atmosphere model. *J. Phys. Oceanogr.,* **37,** 1103–1121.

Bower, A. S., and N. G. Hogg, 1992: Evidence for barotropic wave radiation from the Gulf Stream. *J. Phys. Oceanogr.,* **22,** 42–61.

Cessi, P., 1990: Recirculation and separation of boundary currents. *J. Mar. Res.,* **48,** 1–35.

——, G. Ierley, and W. Young, 1987: A model of the inertial recirculation driven by potential vorticity anomalies. *J. Phys. Oceanogr.,* **17,** 1640–1652.

Cronin, M., 1996: Eddy-mean flow interaction in the Gulf Stream at 68°W. Part II: Eddy forcing on the time-mean flow. *J. Phys. Oceanogr.,* **26,** 2132–2151.

——, and D. R. Watts, 1996: Eddy-mean flow interaction in the Gulf Stream at 68°W. Part I: Eddy energetics. *J. Phys. Oceanogr.,* **26,** 2107–2131.

Dewar, W. K., and J. M. Bane, 1989: Gulf Stream dynamics. Part II: Eddy energetics at 73°W. *J. Phys. Oceanogr.,* **19,** 1574–1587.

Ducet, N., and P.-Y. Le Traon, 2001: A comparison of surface eddy kinetic energy and Reynolds stresses in the Gulf Stream and the Kuroshio Current systems from merged TOPEX/Poseidon and ERS-1/2 altimetric data. *J. Geophys. Res.,* **106,** 16 603–16 622.

Durran, D. R., 1991: The third-order Adams–Bashforth method: An attractive alternative to leapfrog time differencing. *Mon. Wea. Rev.,* **119,** 702–720.

Flierl, G. R., P. Malanotte-Rizzoli, and N. J. Zabusky, 1987: Nonlinear waves and coherent vortex structures in barotropic beta-plane jets. *J. Phys. Oceanogr.,* **17,** 1408–1438.

Fofonoff, N. P., 1954: Steady flow in a frictionless homogeneous ocean. *J. Mar. Res.,* **50,** 545–566.

——, 1981: The Gulf Stream system. *Evolution in Physical Oceanography: Scientific Surveys in Honor of Henry Stommel,* B. A. Warren, Ed., MIT Press, 112–139.

Greatbatch, R. J., 1987: A model for the inertial recirculation of a gyre. *J. Mar. Res.,* **45,** 601–634.

Haidvogel, D. B., and P. B. Rhines, 1983: Waves and circulation driven by oscillatory winds in an idealized ocean basin. *Geophys. Astrophys. Fluid Dyn.,* **25,** 1–63.

Hogg, N. G., 1983: A note on the deep circulation of the western North Atlantic: Its nature and causes. *Deep-Sea Res.,* **30,** 945–961.

——, 1985: Evidence for baroclinic instability in the Gulf Stream recirculation. *Prog. Oceanogr.,* **14,** 209–229.

——, 1988: Stochastic wave radiation by the Gulf Stream. *J. Phys. Oceanogr.,* **18,** 1687–1701.

——, 1992: On the transport of the Gulf Stream between Cape Hatteras and the Grand Banks. *J. Mar. Res.,* **50,** 545–566.

——, 1993: Toward parameterization of the eddy field near the Gulf Stream. *Deep-Sea Res.,* **40,** 2359–2376.

Jayne, S. R., and N. G. Hogg, 1999: On recirculation forced by an unstable jet. *J. Phys. Oceanogr.,* **29,** 2711–2718.

——, and J. Marotzke, 2002: The oceanic eddy heat transport. *J. Phys. Oceanogr.,* **32,** 3328–3345.

——, N. G. Hogg, and P. Malanotte-Rizzoli, 1996: Recirculation gyres forced by a beta-plane jet. *J. Phys. Oceanogr.,* **26,** 492–504.

——, and Coauthors, 2009: The Kuroshio Extension and its recirculation gyres. *Deep-Sea Res. I,* **56,** 2088–2099.

Johns, W. E., 1988: One-dimensional baroclinically unstable waves on the Gulf Stream potential vorticity gradient near Cape Hatteras. *Dyn. Atmos. Oceans,* **11,** 323–350.

Kelly, K. A., M. J. Caruso, S. Singh, and B. Qui, 1996: Observations of atmosphere-ocean coupling in midlatitude western boundary currents. *J. Geophys. Res.,* **101,** 6295–6312.

Lee, T., and P. Cornillon, 1995: Temporal variation of meandering intensity and domain-wide lateral oscillations of the Gulf Stream. *J. Geophys. Res.,* **100,** 13 603–13 613.

Malanotte-Rizzoli, P., 1994: The Gulf Stream system: Dynamics and modeling. *The Oceans: Physiochemical Dynamics and Resources,* S. K. Majumdar et al., Eds., The Pennsylvania Academy of Science, 108–123.

——, N. G. Hogg, and R. E. Young, 1995: Stochastic wave radiation by the Gulf Stream: Numerical experiments. *Deep-Sea Res.,* **42,** 389–423.

Marshall, J., and G. Nurser, 1986: Steady, free circulation in a stratified quasi-geostrophic ocean. *J. Phys. Oceanogr.,* **16,** 1799–1813.

McCalpin, J., and D. B. Haidvogel, 1996: Phenomenology of the low-frequency variability in a reduced-gravity quasi-geostrophic double-gyre model. *J. Phys. Oceanogr.,* **26,** 739–752.

Meacham, S. P., 2000: Low-frequency variability in the wind-driven circulation. *J. Phys. Oceanogr.,* **30,** 269–293.

Mizuta, G., 2010: Rossby wave radiation from an eastward jet and its recirculations. *J. Mar. Res.,* **67,** 185–212.

Pedlosky, J., 1963: Baroclinic instability in two-layer systems. *Tellus,* **15,** 20–25.

——, 1970: Finite-amplitude baroclinic waves. *J. Atmos. Sci.,* **27,** 15–30.

——, 1972: Finite-amplitude baroclinic wave packets. *J. Atmos. Sci.,* **29,** 680–686.

——, 1976: Finite-amplitude baroclinic disturbances in downstream varying currents. *J. Phys. Oceanogr.,* **6,** 335–344.

Plumb, R. A., and R. Ferrari, 2005: Transformed Eulerian-mean theory. Part I: Nonquasigeostrophic theory for eddies on a zonal-mean flow. *J. Phys. Oceanogr.,* **35,** 165–174.

Primeau, F. W., 1998: Multiple equilibria of a double-gyre ocean model with super-slip boundary conditions. *J. Phys. Oceanogr.,* **28,** 2130–2147.

Qui, B., 1995: Variability and energetics of the Kuroshio Extension and its recirculation gyre from the first two years of TOPEX data. *J. Phys. Oceanogr.,* **25,** 1827–1842.

——, 2000: Interannual variability of the Kuroshio Extension system and its impact on the wintertime SST field. *J. Phys. Oceanogr.,* **30,** 1486–1502.

Reverdin, G., P. P. Niller, and H. Valdimarsson, 2003: North Atlantic Ocean surface currents. *J. Geophys. Res.,* **108,** 3002, doi:10.1029/2001JC001020.

Richardson, P. L., 1985: Average velocity and transport of the Gulf Stream near 55°W. *J. Mar. Res.,* **43,** 83–111.

Schmitz, W. J., 1984: Observations of the vertical structure of the eddy field in the Kuroshio Extension. *J. Geophys. Res.,* **89,** 6355–6364.

——, and M. S. McCartney, 1993: On the North Atlantic circulation. *Rev. Geophys.,* **31,** 29–49.

Spall, M. A., 1994: Wave-induced abyssal recirculations. *J. Mar. Res.,* **52,** 1051–1080.

——, 1996: Dynamics of the Gulf Stream/deep western boundary current crossover. Part II: Low-frequency internal oscillations. *J. Phys. Oceanogr.,* **26,** 2169–2182.

Starr, V. P., 1968: *Physics of Negative Viscosity Phenomena.* McGraw-Hill, 256 pp.

Thompson, R. O. R. Y., 1977: Observations of Rossby waves near site D. *Prog. Oceanogr.,* **7,** 1–28.

——, 1978: Reynolds stress and deep counter-currents near the Gulf Stream. *J. Mar. Res.,* **36,** 611–615.

Waterman, S., 2009: Eddy-mean flow interactions in western boundary current jets. Ph.D. thesis, Massachusetts Institute of Technology and Woods Hole Oceanographic Institution Joint Program, 264 pp.

Watts, D. R., K. L. Tracey, J. M. Bane, and T. J. Shay, 1995: Gulf Stream path and thermocline structure near 74°W and 68°W. *J. Geophys. Res.,* **100,** 18 291–18 312.

Whitehead, J., 1975: Mean flow driven by circulation on a beta-plane. *Tellus,* **27,** 358–364.

Xue, H., 1991: Numerical studies of Gulf Stream meanders in the South Atlantic Bight. Ph.D. thesis, Princeton University, 188 pp.